Design of an Efficient Endodontic File Material Utilizing Artificial Intelligence

by

Asiye Nur Şahin

A Dissertation Submitted to the
Graduate School of Sciences and Engineering

in Partial Fulfillment of the Requirements for

the Degree of

Master of Science

in

Mechanical Engineering

KOÇ ÜNİVERSİTESİ

August 1, 2025

Design of an Efficient Endodontic File Material Utilizing Artificial Intelligence

Koç University

Graduate School of Sciences and Engineering

This is to certify that I have examined this copy of a master's thesis by

Asiye Nur Şahin

and have found that it is complete and satisfactory in all respects,

and that any and all revisions required by the final

examining committee have been made.

Committee Members:

Prof. Demircan Canadinç (Advisor)

Prof. Murat Sözer

Assoc. Prof. S. Mine Toker

Date: ____

ABSTRACT

MSc Thesis Title
Asiye Nur Şahin
Master of Science in Mechanical Engineering
August 1, 2025

Nickel-titanium (NiTi) alloys have led to a revolutionary development in endodontics due to their flexibility and shape-memory properties. However, despite this advancement, one of the most critical issues limiting the clinical success of NiTi rotary instruments is their fracture within the root canal. The most common cause of these fractures is the material's limited resistance to cyclic fatigue. In this study, machine learning was utilized to determine the ideal NiTi composition that would maximize the cyclic fatigue resistance of NiTi rotary instruments. For this purpose, thermal and structural properties were first obtained through SEM-EDX and DSC analyses conducted on various commercial endodontic files, and these features were included as inputs in the model. Feature selection was performed using Pearson Correlation Coefficient (PCC) and Random Forest (RF) importance-based ranking methods. Subsequently, six different regression algorithms (RF, GBDT, SVR, LR, KNN, XGB) were trained, and their performances were evaluated using R^2, RMSE, and MAE criteria. Preprocessing steps, including outlier detection, standardization, and 10-fold cross-validation, were applied to the dataset. As a result of analyses conducted using a stepwise feature addition strategy, the highest generalization performance was achieved with the K-Nearest Neighbors (KNN) and Support Vector Regression (SVR) models. To evaluate the effect of training/test ratios, various data splitting scenarios were tested, an 10% testing ratio was determined to be optimal. Using the best-performing model, synthetic NiTi compositions were generated in the range of 48–57 at % Ni with a resolution of 0.03 at.%. Based on the predictions, the three compositions with the highest NCF values were identified and selected for experimental validation. The results obtained demonstrate the effectiveness of machine learning in material design and contribute to the development of next-generation endodontic instruments.

ÖZETÇE

Yüksek Lisans Tez Başlığı
Asiye Nur Şahin
Makine Mühendisliği, Yüksek Lisans
1 Ağustos 2025

Nikel-titanyum (NiTi) alaşımları, esneklikleri ve şekil hafızalı özellikleri sayesinde endodontide devrim niteliğinde bir gelişme yaratmıştır. Ancak bu ilerlemeye rağmen, NiTi döner aletlerin klinik başarısını sınırlayan en önemli sorunlardan biri, kanal içinde kırılmalarıdır. Bu kırılmaların en yaygın nedeni, malzemenin döngüsel yorgunluk karşısındaki sınırlı direncidir. Bu çalışmada NiTi döner aletlerin döngüsel yorgunluk dayanımını maksimize edecek ideal NiTi kompozisyonunu belirlemek amacıyla makine öğrenmesinden yararlanılmıştır. Bu amaç doğrultusunda öncelikle, çeşitli ticari endodontik eğelerde yapılan SEM-EDX ve DSC analizleri ile termal ve yapısal özellikler elde edilmiş ve modele girdi olarak dahil edilmiştir. Özellik seçimi için Pearson Korelasyon Katsayısı (PCC) ve Random Forest (RF) temelli önem sıralaması yöntemleri kullanılmış; ardından altı farklı regresyon algoritması (RF, GBDT, SVR, LR, KNN, XGB) eğitilerek performansları R^2, RMSE ve MAE kriterlerine göre değerlendirilmiştir. Veri setine anormallik tespiti, standardizasyon ve 10 katlı çapraz doğrulama gibi ön işleme adımları uygulanmıştır. Adım adım özellik ekleme stratejisiyle yapılan analizler sonucunda, en yüksek genelleme performansının K-Nearest Neighbors (KNN) ve Support Vector Regression (SVR) modelleriyle elde edildiği görülmüştür. Eğitim/test oranlarının etkisini değerlendirmek amacıyla farklı veri bölme senaryoları test edilmiş ve %90 eğitim / %10 test oranının optimal olduğu belirlenmiştir. En iyi model ile, 48–57 at.% Ni aralığında 0.03 at.% çözünürlükle oluşturulan sentetik NiTi bileşimlerinden elde edilen tahminler doğrultusunda en yüksek NCF değerini veren üç kompozisyon belirlenmiş ve deneysel doğrulama için seçilmiştir. Elde edilen sonuçlar, malzeme tasarımında makine öğrenmesinin etkinliğini göstermekte ve yeni nesil endodontik alet geliştirme sürecine katkı sağlamaktadır.

AKNOWLEDGEMENTS

I would like to express my sincere gratitude to my dear advisor, Prof. Demircan Canadinç, for encouraging me from the very beginning of this journey, for always being there with his guidance, and for helping me make one of my dreams come true.

I sincerely thank Prof. Dr. Murat Sözer and Assoc. Prof. Dr. S. Mine Toker for their valuable contributions as members of my thesis committee.

I am also grateful to Prof. Hans Jürgen Maier and Christian Hinte for their support during the experimental phase of this study.

I would like to thank Azizeh, whose contribution was especially significant, for patiently guiding me through many topics that were completely new to me. I also thank Aysu and Alireza for their support.

To my dear mother, who accompanied me on campus and took care of my daughter while I studied, and to all my family.

To my beloved husband, Onur Can, thank you for always being by my side. I know none of this would have been possible without your endless support.

And of course, to my precious Ayla. I'm sure this thesis could have been completed much sooner without you, but I'm not sure it would have been this meaningful.

Finally, I sincerely thank all my loved ones who make me say to myself, "I'm a truly lucky person."

TABLE OF CONTENTS

LIST OF TABLES

LIST OF FIGURES

ABBREVIATIONS

A_s	Austenite Start
A_f	Austenite Finish
CM	Controlled Memory
CV	Cross-validation
DSC	Differential Scanning Calorimetry
EDM	Electrical Discharge Machining
GBDT	Gradient Boosted Decision Trees
KDE	Kernel Density Estimate
KNN	K-Nearest Neighbors
LR	Linear Regression
MAE	Mean Absolute Error
M_f	Martensite Finish
MR	Martensite Reorientation
M_s	Martensite Start
NCF	Number of Cycles to Failure
NiTi	Nickel Titanium
PCC	Pearson Correlation Coefficient
R^2	Coefficient of Determination
R_f	Rhombohedral Finish Temperature
RF	Random Forests
RMSE	Root Mean Squared Error
R_s	Rhombohedral Start Temperature
SEM-EDX	Scanning Electron Microscopy with Energy Dispersive X-ray Spectroscopy
SIM	Stress-induced Martensite
SS	Stainless Steel
SVR	Support Vector Regression
TTR	Transformation Temperature Range
XGB	Extreme Gradient Boosting

Chapter 1:
INTRODUCTION

Root canal preparation is a fundamental step in endodontic treatment, directly influencing both the cleaning efficacy and the long-term success of therapy. In pursuit of more efficient and safer instrumentation, the introduction of nickel-titanium (NiTi) rotary files marked a pivotal development in the field. Due to their superior elasticity and shape memory compared to stainless steel, NiTi instruments enable safer navigation of curved canals with reduced risk of procedural errors [1].

Despite these advantages, instrument separation during canal preparation remains a major clinical concern [2]. One of the leading causes of such fractures is cyclic fatigue, which occurs when the instrument undergoes repeated tensile and compressive stresses, especially in curved canals, leading to internal crack propagation and failure. Cyclic fatigue fractures are often unpredictable because they typically occur without visible signs of deformation [3, 4].

To address this issue, extensive research has focused on improving the fatigue resistance of NiTi instruments. Advances in thermomechanical processing have resulted in heat-treated alloys with modified phase transformation behaviors, such as martensitic or R-phase dominance, enhancing flexibility and fatigue life [4]. Among the various contributing factors, the metallurgical composition of the NiTi alloy plays a key role in determining the instrument's mechanical performance, particularly its resistance to cyclic fatigue [5]. While several studies have quantified the cyclic fatigue behavior of different NiTi instruments, no study has systematically analysed this data to determine the ideal alloy formulation for maximum fatigue resistance.

This study aims to address that gap by collecting cyclic fatigue data from the literature and combining it with experimental results obtained through Differential Scanning Calorimetry (DSC) and Scanning Electron Microscopy with Energy Dispersive X-ray Spectroscopy (SEM-EDX). Machine learning models, including Random Forest (RF), Gradient Boosted Decision Trees (GBDT), Support Vector Regression (SVR), Linear

Regression (LR), K-Nearest Neighbors (KNN), and Extreme Gradient Boosting (XGB), are applied to predict the most effective NiTi composition for fatigue resistance.

The thesis starts with a literature review to provide background information. It then proceeds with the presentation of experimental data acquired through SEM-EDX and DSC analyses. Following this, the machine learning approach used for modelling and prediction is described. The thesis concludes with a discussion of the results, conclusions, and suggestions for future research.

1.1 Root Canal Anatomy and Mechanical Instrumentation

Root canal anatomy forms the foundation of the art and science of endodontic treatment. The human dentition exhibits significant anatomical diversity across various tooth types [6]. Nevertheless, each tooth is fundamentally composed of four main tissues: enamel, which envelops the crown; dentin, forming the bulk of both the crown and root; cementum, which covers the root surface and interfaces with enamel at the cervical region; and pulp tissue, which occupies the central pulp chamber and root canals within the dentin. The crown refers to the part of the tooth extending above the gingival margin and covered by enamel, whereas the root is embedded within the alveolar bone of the jaws [7] (Figure 1.1)

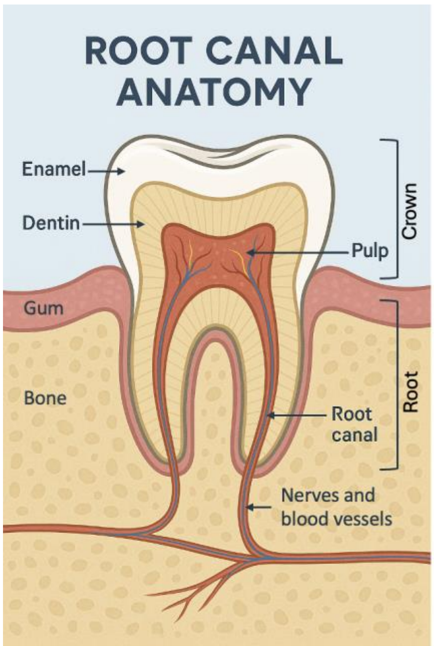

Figure 1.1 Anatomy of the tooth

Because root canal anatomy is complex and varies significantly between teeth, each case requires an individualized and careful treatment approach. Root canal treatment consists of several key steps. First, following a comprehensive clinical and radiographic evaluation, a definitive diagnosis is established and an appropriate treatment plan is formulated. Next, any existing carious tissue or defective restorations are removed. After localization of the canal orifices, working length determination is performed using electronic and/or radiographic methods. Root canal shaping is achieved through mechanical instrumentation in conjunction with effective irrigation protocols. Subsequently, the cleaned and shaped canals are obturated using a biocompatible material to ensure three-dimensional sealing. The treatment is finalized with a coronal restoration, either a direct filling or an indirect restoration, to prevent reinfection and maintain tooth integrity.

A critical phase of this procedure is mechanical preparation. The objective of root canal preparation is to facilitate the disinfection and obturation of the root canal space. Preparation develops a tapered shape from the orifice to provide apical resistance form during obturation [8, 9]. This shaping process is carried out using a range of instruments specifically designed for root canal preparation. All instruments generally referred to as *files* are those that are manually operated. To use files effectively, the clinician should understand the components of each file and how design differences influence their performance. *Taper* is typically defined as the amount by which the file's diameter increases per millimeter from the tip toward the handle. For instance, a size #25 file with a .02 taper will have a diameter of 0.27 mm at 1 mm from the tip, 0.29 mm at 2 mm, and 0.31 mm at 3 mm. Some manufacturers represent taper as a percentage; for example, a .02 taper equals a 2% taper. The *flute* of a file is the groove along the working surface that collects soft tissue and dentin debris removed from the canal walls. The part of the file with the largest diameter that follows this groove (where the flute meets the land) creates the *cutting edge*, also known as the blade of the file [10] (Figure 1.2). In addition to understanding the structural features of files, it is also beneficial to review the evolution of endodontic instruments over time.

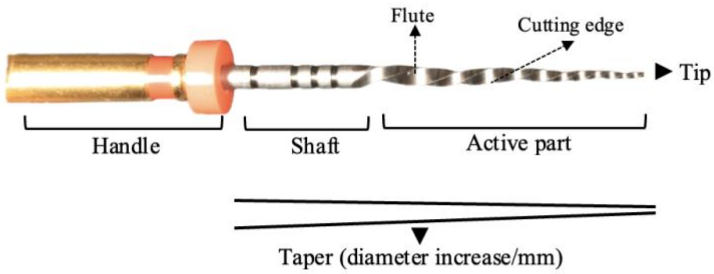

Figure 1.2 Main components of an endodontic file

1.2 *Histological Development of NiTi Instruments in Endodontics*

Historically, root canal instruments were manufactured from carbon steel. Later, the use of stainless steel (SS) significantly improved their quality. More recently, the introduction of nickel-titanium alloy in endodontic instrument manufacturing has led to major advancements in canal shaping [10].

Buchanan [11] is one of the authors who best summarized the impact of NiTi rotary instruments in endodontics. According to him, the introduction of NiTi rotary files changed almost everything in the field: the approach, the technique, and even the economics. These instruments made root canal treatment more accessible and even enjoyable for dentists. Although NiTi files are more expensive than traditional stainless steel hand files, they offer better performance, which has made them widely accepted.

The use of NiTi alloy for shaping root canals marked a major step forward in endodontics. With advancements in NiTi metallurgy, new instruments with innovative designs were developed, improving both effectiveness and efficiency. In summary, shaping root canals with NiTi rotary instruments is more predictable, simpler, and more comfortable for clinicians compared to manual preparation with SS hand files [12].

The NiTi alloy was originally developed in the United States by William Buehler in 1963. It was initially named NiTiNOL, a name derived from its components, nickel (Ni) and titanium (Ti), along with the Naval Ordnance Laboratory (NOL) where it was created [13]. In the field of dentistry, Andreasen and Morrow [14] were the first to introduce NiTiNOL in orthodontic applications, recognizing its low elastic modulus, shape memory properties, and exceptional flexibility. Later, in 1975, Civjan *et al.* [15] published a paper proposing the potential use of this alloy across various dental disciplines, including endodontics.

By the early 1990s, NiTi rotary files became available for commercial use. Since then, these instruments have undergone continuous development and are now categorized into five generations based on their design features, manufacturing techniques, and metallurgical advancements [16].

1.2.1 First generation

The first .02 taper NiTi rotary instrument was introduced in 1992 by Dr. John McSpadden. While these tools marked a shift in how clinicians approached root canal instrumentation, they also presented notable challenges, particularly a high risk of instrument fracture. One major limitation of this first generation was the need for multiple files to complete canal shaping, along with complicated and time-consuming clinical protocols. The elevated fracture rate, especially when compared to manual techniques, was likely due to both limitations in early manufacturing quality and insufficient understanding among clinicians about how to safely use these new instruments [12, 16].

1.2.2 Second generation

Starting in the late 1990s, manufacturers began focusing on creating safer and more effective rotary instruments by modifying their surface characteristics, such as through electropolishing and ion implantation, and altering design elements like helical angles, tapers, and cutting edges. These refinements in manufacturing techniques, combined with increased clinician experience, led to noticeable improvements in the performance of the second-generation NiTi rotary files. However, despite these advancements, instrument fracture remained a significant issue [12].

1.2.3 Third generation

The third generation of NiTi rotary instruments is defined by significant advancements in alloy metallurgy, particularly the introduction of heat treatment techniques. These thermal processing methods were aimed at modifying the transition temperatures of NiTi alloys, which in turn enhanced the flexibility and fatigue resistance of the instruments [16]. Beginning around 2007, manufacturers started applying proprietary thermomechanical treatments to their files, each developing unique and patented approaches. This evolution in manufacturing led to files with improved mechanical properties, offering greater safety and enhanced shaping performance, especially in anatomically challenging cases such as curved root canals. The refinement of the alloy’s crystalline structure through heat treatment became a key factor in reducing the risk of fracture and boosting overall clinical efficiency [12, 17].

1.2.4 Fourth generation

The majority of endodontic shaping instruments in clinical use today are made from NiTi alloy and operate using continuous rotary motion [16]. However, building on the metallurgical advancements of the previous generation, the fourth generation introduced a significant innovation in the form of new kinematics, specifically the shift from continuous rotation to reciprocating motion. This technique involves a larger counterclockwise rotation for dentin cutting and a smaller clockwise rotation to reduce stress on the instrument, thereby minimizing the risk of fracture [12]. In 2008, Dr. Ghassan Yared [18] pioneered this method by determining the exact unequal clockwise and counterclockwise angles that made it possible to shape almost any root canal with a single 25/0.08 file using reciprocating motion.

1.2.5 Fifth generation

The fifth and most recent generation of NiTi instruments features advanced metallurgical treatments along with significant changes in the geometry of the cutting blades. These instruments are designed with an offset center of mass and/or center of rotation, enabling eccentric or asymmetric motion during canal shaping. This off-centered design improves cutting efficiency and reduces the screw-in effect, contributing to safer and more effective instrumentation [12, 16].

1.3 Thermomechanical Behavior of NiTi Instruments in Endodontics

NiTi, known as a shape memory metal alloy, can exist in two distinct temperature-dependent crystal structures: martensite (the low-temperature or daughter phase) and austenite (the high-temperature or parent phase) [19]. The crystal lattice can change in response to either temperature or mechanical stress, which is significant because the two phases have notably different properties. Near-equiatomic NiTi alloys may contain three microstructural phases: Austenite, martensite, and R-phase. The characteristics and proportions of these phases determine the material's mechanical behavior. In the martensitic state, NiTi is soft and ductile and can be easily deformed, whereas in the austenitic state, it is much stronger and harder [20].

In a typical tensile stress-strain curve of an equiatomic NiTi alloy, mechanical behavior can be described in eight stages based on three primary deformation mechanisms: stress-induced martensitic (SIM) transformation, martensite reorientation (MR), and plastic deformation (Figure 1.3). When external stress is applied to the austenitic phase of the NiTi alloy, it transforms into martensite (SIM – Stage IV). During this transformation, the stress remains nearly constant while strain increases. This region corresponds to superelastic behavior, where the material returns to its original shape upon unloading. If the material is already in the martensitic phase, the applied stress causes reorientation of martensitic variants (MR - Stage VI). This deformation is recoverable upon heating, and it is associated with the shape memory effect. Beyond a specific strain, the material no longer deforms through phase transformation or reorientation. Instead, it undergoes permanent plastic deformation (Stage VIII), which is irreversible. Additionally, a transitional phase may appear before the austenite-to-martensite transition (Stages II–III). It allows for limited strain recovery (approximately 0.5%) and exhibits a very narrow thermal hysteresis. The SIM mechanism is responsible for superelasticity, whereas the MR mechanism explains the shape memory effect. Compared to stainless steel, which only has a strain of less than 1%, NiTi's superelasticity enables the complete recovery of deformations with strain values up to 8% [4].

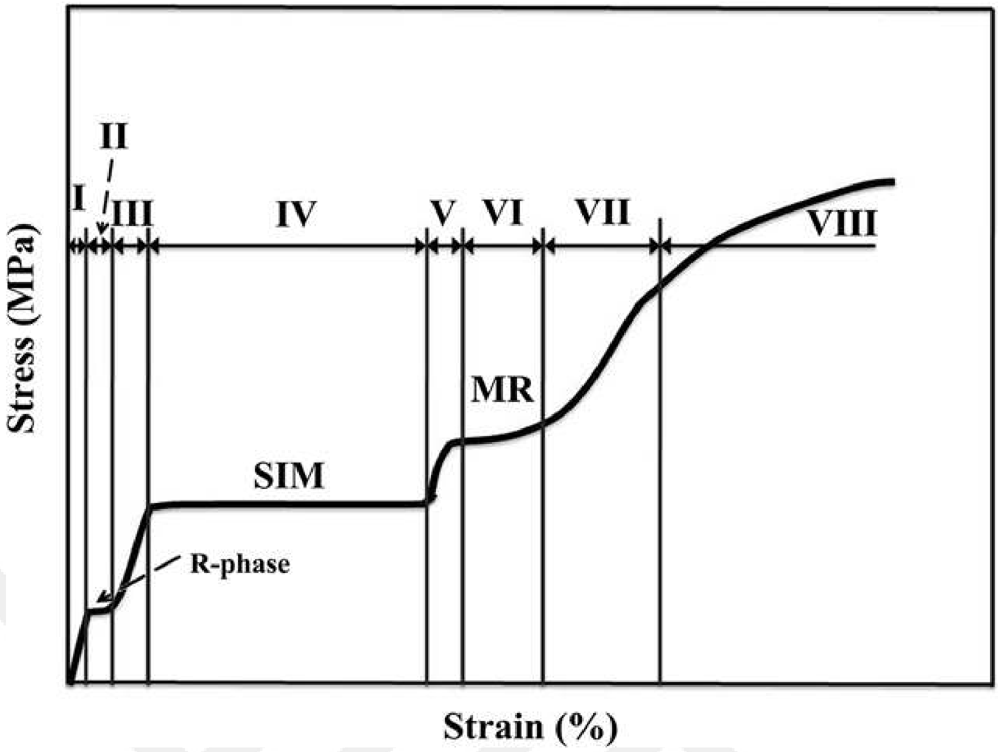

Figure 1.3 Stress-strain curve of an equiatomic NiTi alloy [4]

Numerous conventional NiTi endodontic files, such as ProTaper Universal, Mtwo, and OneShape, are made from superelastic NiTi alloys. These instruments operate in the austenitic phase under clinical (i.e., body temperature) conditions [21-23].

Another type of mechanical deformation in NiTi alloys is martensite variant reorientation, which is associated with the shape memory effect. When NiTi is deformed in its martensitic state, it undergoes a strain that can be fully recovered by heating. This phenomenon is referred to as the shape memory effect. Such deformation through variant reorientation typically occurs at temperatures below austenite start (A_s), the critical temperature at which reverse transformation to austenite begins, and is completed at austenite finish (A_f). This process is thermally activated and depends on the alloy's transformation temperatures [4, 24] (Figure 1.4).

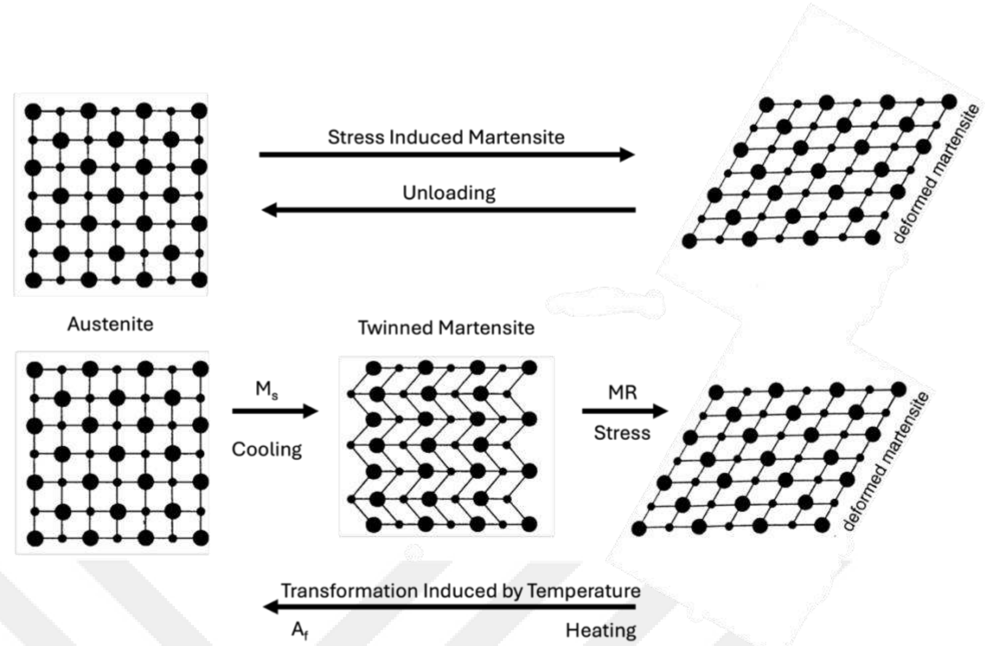

Figure 1.4 Schematic representation of phase crystallographic transformation of NiTi alloy induced by stress or temperature variation [25].

The martensite phase of NiTi is a low-temperature phase with a monoclinic (B19′) structure, and it exhibits a lower Young's modulus (20–50 GPa) and yield strength (~138 MPa) compared to austenite (40–90 GPa and ~379 MPa, respectively). This means martensite can deform more easily under low stress, whereas austenite requires much higher stress for deformation. In addition to being more flexible, martensite reduces the risk of file fracture under stress because it can undergo plastic deformation instead of fracturing. To enhance mechanical properties, martensitic characteristics have been introduced into commercial NiTi endodontic instruments like M-wire and CM-wire systems [4].

1.4 *Cyclic Fatigue of NiTi Endodontic Files*

With the continuous introduction of new products to the market, numerous studies have also been conducted in this field. These studies mainly focus on flexibility, cutting efficiency, fracture resistance, and bending properties [26].

Instrument fractures can occur due to several factors, such as the clinician's experience, rotation speed, number of uses, presence of a glide path, canal curvature angle and radius, sterilization procedures, the type of irrigation solution used, instrument design and metallurgy [26, 27].

Instrument fractures primarily occur due to torsional stress, cyclic fatigue, or a combination of both. As a result, many studies focus on how instruments behave under these conditions. The basic testing standards for endodontic files are described in the updated ADA Specification No. 28 and ISO 3630-1:2008. However, to date, there is no specific guideline or international standard for testing the cyclic fatigue or torsional resistance of rotary endodontic instruments [26, 28].

Torsional fracture occurs when the tip of an instrument is firmly engaged in a root canal. At the same time, the endodontic motor continues to rotate or reciprocate, exceeding the shear strength of the instrument. This happens because the friction between the instrument and the root canal dentin increases the rotational torque load beyond the instrument's torsional strength, leading to failure [26, 29].

Cyclic fatigue happens due to repeated tensile and compressive stress. When an endodontic instrument rotates in a curved canal, it is exposed to both types of stress in the curved area. The curved shape causes the instrument to bend, leading to internal stress. The outer side of the curve is under tension, while the inner side is under compression. With each rotation, the instrument goes through a complete cycle of tension and compression. This repeated stress is the most damaging form of cyclic loading. Generally, resistance to cyclic fatigue is measured as time to fracture or the number of cycles (NCF) [30]. It has been stated that the clinical relevance of cyclic fatigue tests is difficult to assess, as laboratory conditions differ from actual clinical situations where various factors, including torsional stress, contribute to instrument fracture [31]. However, such laboratory studies are still considered useful for evaluating a single parameter, like cyclic fatigue, under standardized conditions [26], and most cyclic fatigue tests have been conducted using the experimental setups described below

Cyclic fatigue is typically investigated using static test setups in most experimental studies. Metal blocks simulating the root canal are commonly used (Figure 1.5). Although studies have shown that temperature can affect cyclic fatigue resistance, most experiments were performed under room temperature conditions [32, 33].

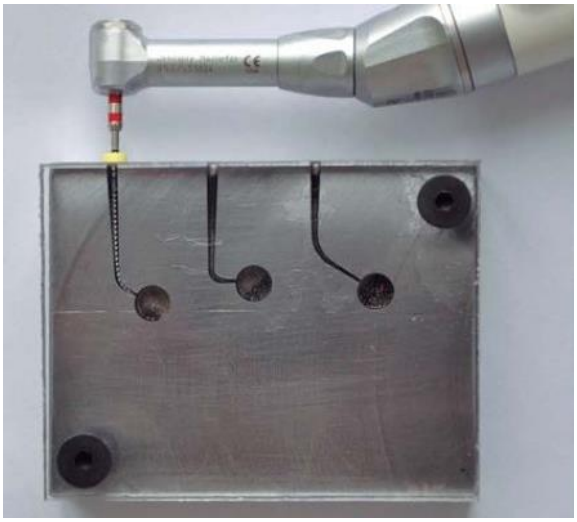

Figure 1.5 Cyclic fatigue testing device [34]

Canal curvature was initially defined by Schneider, and his definition includes only a single parameter, which is the angle of curvature [35]. Later on, Pruett et al. improved this definition by adding the radius of curvature, providing a more precise description [30]. (Figure 1.6). Therefore, when describing the curvature of the experimental setup in such studies, both the angle and the radius of curvature are typically reported.

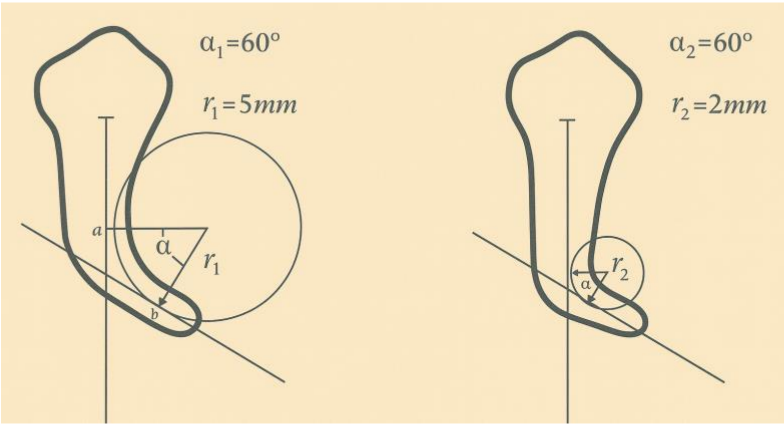

Figure 1.6 Radius and angle of curvature [30]

Several instrument-related parameters have been identified as potential contributors to cyclic fatigue behavior. It is known that file design affects fracture resistance. One of the key design parameters is the cross-sectional shape of the file. When examining the files produced so far, various cross-sectional designs can be seen, such triangular, parallelogram, S-shaped, and square. In a study by Di Nardo et al., files with the same heat treatment, apical diameter, and taper but different cross-sectional designs were compared in terms of fracture resistance, and it was concluded that cross-sectional shape is an important factor [36]. The cross-sectional features of fifth-generation file systems are designed with asymmetric mass and center of rotation. This design helps minimize the contact between the file and dentin, which has a positive effect on cyclic fatigue resistance. The larger the metal mass at the point of maximum stress, the lower the fatigue resistance [37].

Another important component in file design is the apical diameter and taper. When comparing files with the same apical diameter but different taper, those with a greater taper are less resistant to fracture [38]. Taper plays a more critical role compared to apical diameter, and both increased taper and apical size can negatively affect cyclic fatigue performance [5].

Chapter 2:
THERMAL AND MICROSTRUCTURAL ANALYSIS OF SELECTED INSTRUMENTS

2.1 *Differential Scanning Calorimetry Analysis*

The transformation of NiTi alloys between different phases is typically associated with a slight temperature shift. For instance, the transition from austenite to martensite is accompanied by a slight release of thermal energy, whereas the reverse transformation (from martensite to austenite) is an endothermic process that absorbs heat. The enthalpy change associated with these transitions can be accurately measured by Differential Scanning Calorimetry (DSC), a standard technique used for the thermal characterization of NiTi materials. In this method, both the sample and an inert reference are heated at the same rate, and the difference in thermal energy input is precisely monitored. Phase transformations are detected as endothermic peaks on the heating curve and exothermic peaks on the cooling curve. The extent to which the transformation temperatures differ from the ambient or working temperature plays a critical role in determining the thermal stability of the phases present in the material [28].

The Transformation Temperature Range (TTR) is a key characteristic of NiTi alloys, used to define the temperature range within which the material functions effectively. TTR is the temperature range (−120 ℃ to 200 ℃) where the martensite and austenite phases of NiTi alloy coexist and can transform into each other. The martensite start temperature (M_s) marks the onset of martensite formation, while the martensite finish temperature (M_f) is the point at which the transformation to martensite is complete. Upon heating, the reverse transformation begins at the austenite start temperature (A_s) and completes at the austenite finish temperature (A_f). Accordingly, the martensite phase is stable below the TTR, and the austenite phase is stable above it. The transformation between the martensite phase and the austenite phase may occur in two steps, involving the intermediate R-phase, which forms upon cooling through the rhombohedral start temperature (Rs) and completes at the rhombohedral finish temperature (Rf)[39].

The phase transformation behavior of endodontic NiTi rotary instruments is closely related to their austenite finish temperature (Af), which determines the dominant phase under clinical conditions. Instruments with Af values well below room temperature remain fully austenitic at both room and body temperatures (~37°C), leading to increased stiffness and cutting efficiency, but reduced resistance to cyclic fatigue. In contrast, instruments with A_f values above body temperature maintain a martensitic or mixed-phase structure during clinical use, offering greater flexibility and improved fatigue resistance. Instruments with A_f values near body temperature may display intermediate mechanical properties due to partial phase transformation or the presence of the R-phase [40].

In this study, DSC analysis was performed on a 3 mm segment obtained from 10 mm from the tip. The sample was heated from room temperature to 100°C, cooled to –80°C, and then reheated (Figure 2.1). Transformation temperatures (M_s, M_f, M_p, A_s, A_f, A_p) and enthalpy values (Ham, Hma) were identified during the thermal cycle (Table 2.1**).** Notably, data for the ProTaper Universal system, which is no longer in production, was derived from published literature rather than experimental analysis and should be interpreted with that context in mind [41].

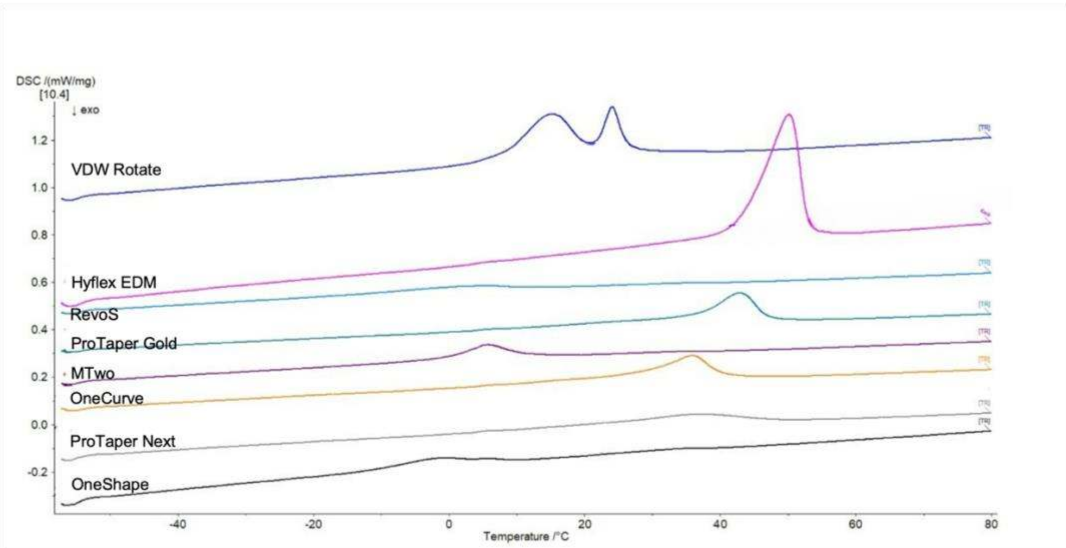

Figure 2.1 DSC thermograms of various NiTi endodontic instruments.

Table 2.1 Phase transformation temperatures and enthalpy values for tested NiTi rotary instruments.

File	Ms [°C]	Mp [°C]	Mf [°C]	Ham [J/g]
RevoS	8,7	-4,3	-15,6	-1,562
VDW Rotate	21	17,1	14,7	-3,72
ProTaper Gold	42	35,6	30,4	-4,594
MTwo	9,1	-1,2	-6,7	-2,798
OneCurve	35,9	30	23	-4,233
ProTaper Next	40,6	32,2	23,5	-2,324
OneShape	2,9	-7,3	-14,7	-1,813
Hyflex EDM	45,5	40,8	36,9	-5,905
	-5,3	-12	-21,3	-9,018
File	**As [°C]**	**Ap [°C]**	**Af [°C]**	**Hma [J/g]**
RevoS	-10	5,5	9,8	1,421
VDW Rotate	8,4	15,4	26,2	13,22
ProTaper Gold	36,9	42,7	46,8	4,382
MTwo	0,6	5,7	10,6	2,964
OneCurve	29,2	35,7	39,9	4,785
ProTaper Next	28,2	37,2	45,5	2,337
OneShape	-12,5	-0,8	6,9	2,469
Hyflex EDM	42,9	50,1	53	19,9
ProTaper Universal	-7		11	

2.2 *Scanning Electron Microscopy (SEM) and Energy Dispersive X-ray Spectroscopy (EDX) Analysis*

EDX is an analytical method employed for elemental or chemical characterization of a sample. In this context, it was used to identify the elemental composition of the NiTi alloy semi-quantitatively and to detect any surface deposits present on the instruments [42].

The same endodontic files were also subjected to scanning electron microscopy (SEM, Zeiss Supra 55 VP) and energy-dispersive X-ray (EDX) analysis (Bruker AXS GmbH, Karlsruhe, Germany) (Figure 2.2).

Elemental composition was evaluated on the cross-sectional surface, at a distance of 10 mm from the tip (Table 2.2). The elemental composition of ProTaper Universal was not measured in this study and was obtained from a previously published source, [43].

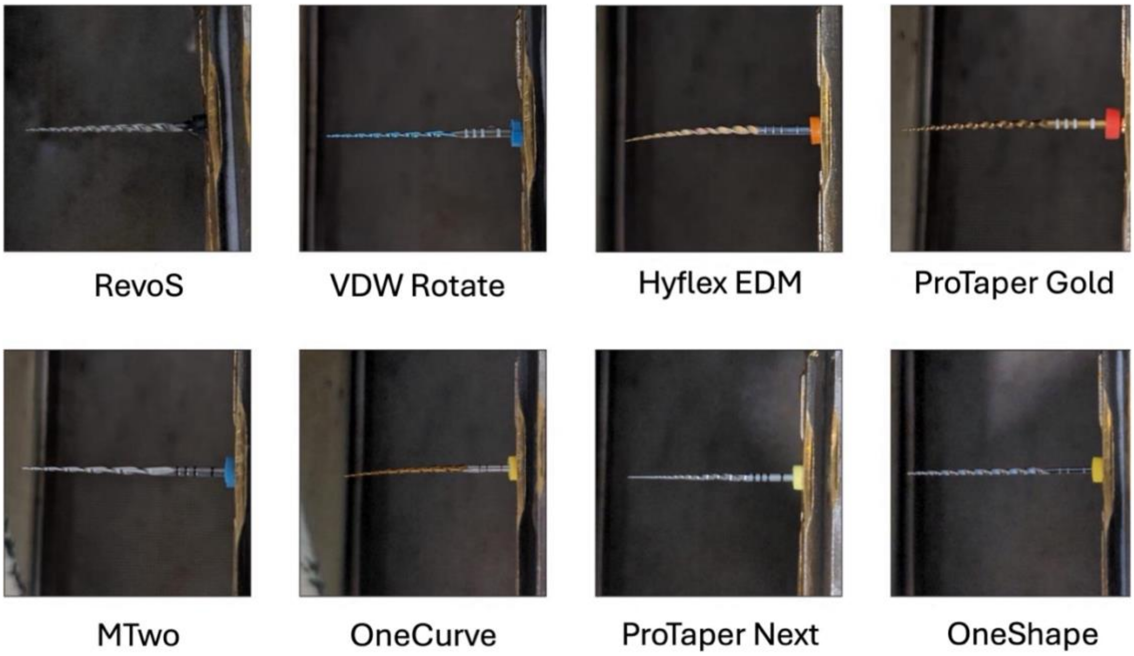

Figure 2.2 NiTi rotary instruments analyzed by SEM-EDX in this study

Table 2.2 The elemental composition (at%) of tested files.

File	**Ti (%)**	**Ni (%)**
Hyflex EDM	51.47	48.53
OneShape	51.13	48.87
ProTaper Next	51.25	48.75
OneCurve	51.42	48.58
MTwo	51.25	48.75
ProTaper Gold	51.38	48.62
VDW Rotate	51.46	48.54
Revo-S	51.49	48.51
ProTaper Universal	50.55	49,45

2.2.1 OneShape (MicroMega, Besançon, France)

OneShape SU is a conventional NiTi instrument introduced by MicroMega (Besançon, France) in 2011 as the first single-file rotary system designed for continuous rotation. It features a size 25/.06 file with a passive tip and a variable cross-sectional design. The instrument is characterized by three distinct cross-section zones: the apical portion has a triple-helical, the coronal region displays an italic S-shaped cross-section, and a gradual transition exists between these areas [23, 44].

Microstructural analysis of the cross-sectional SEM images revealed two consistent features across several NiTi rotary instruments (Figure 2.3). First, dark-toned regions were identified near the cutting edge and surface areas. These regions were confirmed by EDX to be associated with carbon enrichment. These regions may indicate contamination or residues from polishing, sectioning, or surface treatment processes. Second, multiple dark precipitates were visible within the internal matrix of the instruments. Based on their morphology and distribution, these precipitates were identified as Ti_2Ni intermetallic phases. The presence of Ti_2Ni precipitates in the cross-sectional microstructure of some NiTi rotary instruments may be attributed to a slight titanium-rich composition [45]. These intermetallic phases tend to form as a result of phase separation and can negatively influence the instrument's fatigue resistance [46].

According to DSC analysis, One Shape file's austenite finish temperature is 6,9 °C. SEM-EDX analysis revealed that the file consists of approximately 48,87 % nickel and 51,13% titanium by atomic composition (Figure 2.4)

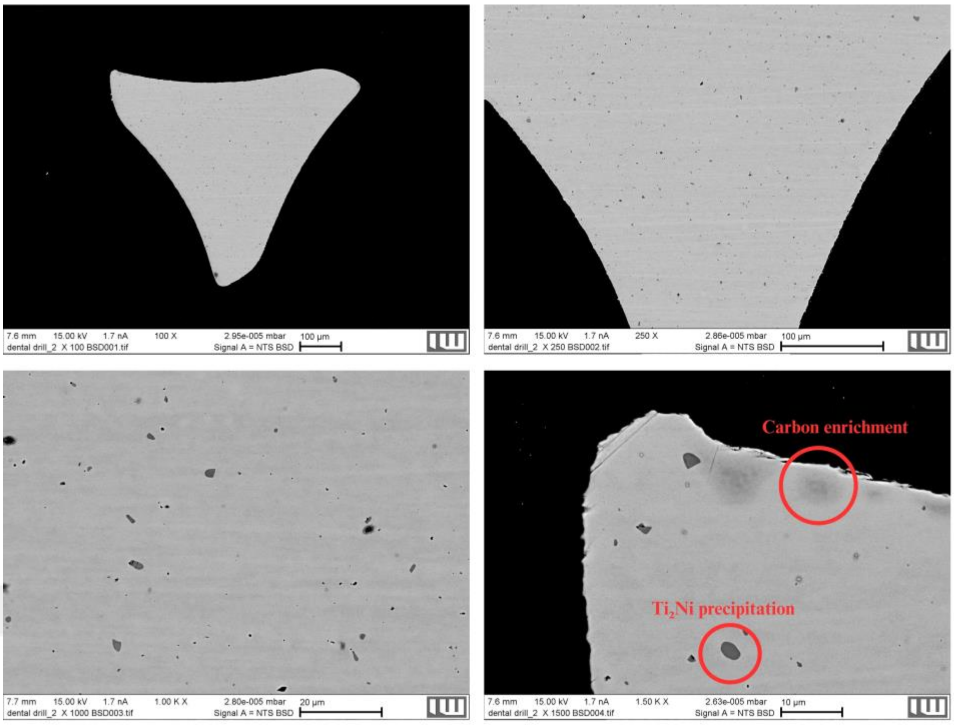

Figure 2.3 SEM images of OneShape file cross-section at increasing magnifications. Microstructural observations include surface-level carbon enrichment and internal Ti_2Ni precipitates, both marked in the highest-magnification image.

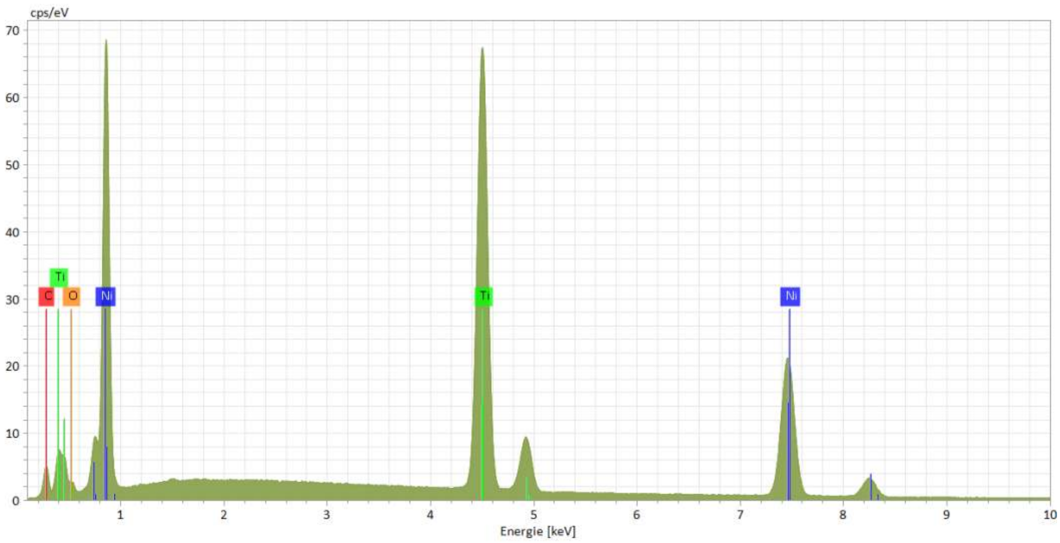

Figure 2.4 EDX result of OneShape

2.2.2 *OneCurve (MicroMega, Besançon, France)*

OneCurve instruments, developed by MicroMega (Besançon, France), were introduced as an enhanced version of the original OneShape system (Figure 2.5). While preserving the same design features as OneShape, these files undergo a proprietary heat treatment process known as C-Wire, which provides greater flexibility and improved shape memory, allowing the instrument to be pre-bent before insertion in the canal [23]. According to DSC analysis, its austenite finish temperature is 39,9 °C. SEM-EDX analysis revealed that the file consists of approximately 48,58 % nickel and 51,42 % titanium by atomic composition (Figure 2.6).

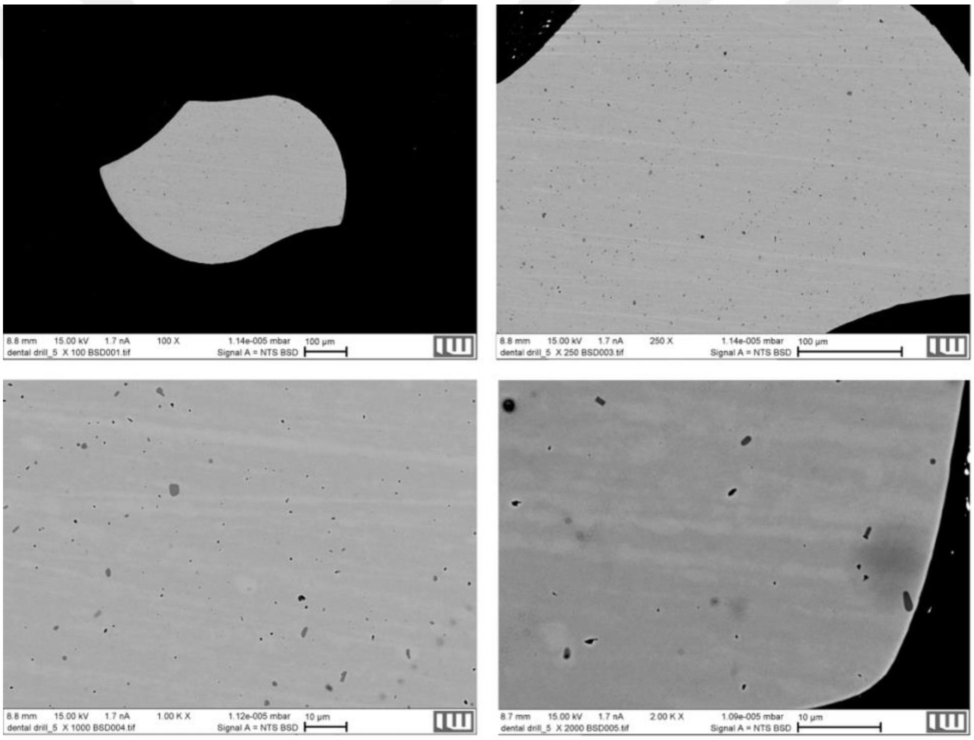

Figure 2.5 SEM images of OneCurve file cross-section at increasing magnifications.

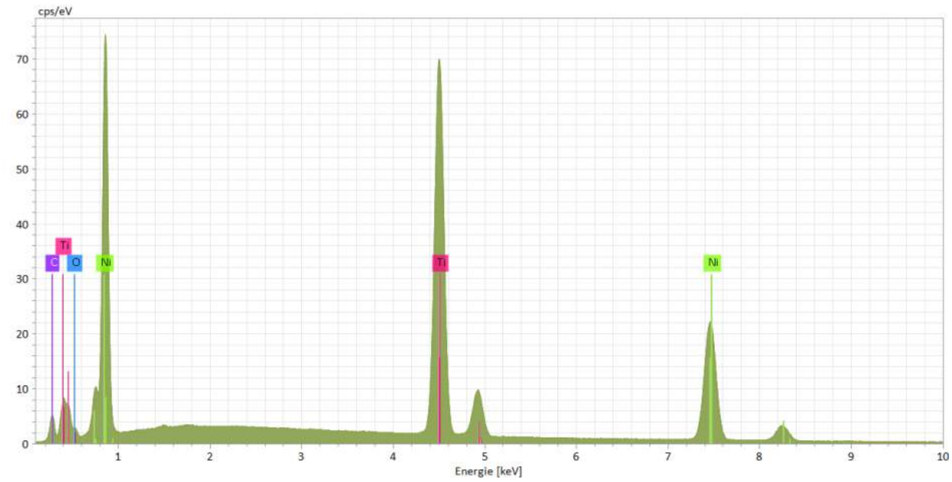

Figure 2.6 EDX result of OneCurve

2.2.3 RevoS (MicroMega, Besançon, France)

Revo-S with SU file was used in this study. Revo-S is a conventional NiTi file and features an asymmetric cross-section and three cutting edges (Figure 2.7). It has an apical diameter of 0.25 mm with a 6% taper [47]. According to DSC analysis, its austenite finish temperature is 9,8 °C. SEM-EDX analysis revealed that the file consists of approximately 48,51 % nickel and 51,49 % titanium by atomic composition (Figure 2.8).

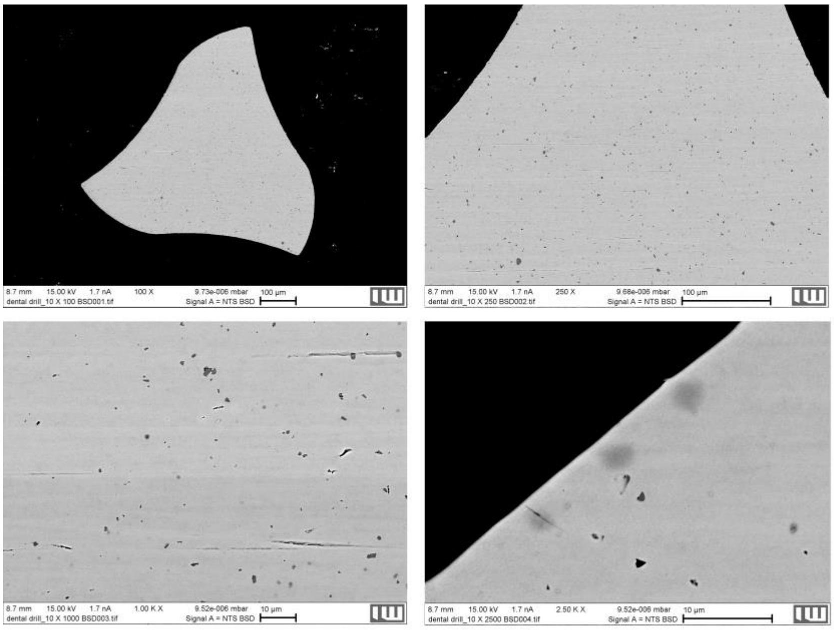

Figure 2.7 SEM images of RevoS file cross-section at increasing magnifications

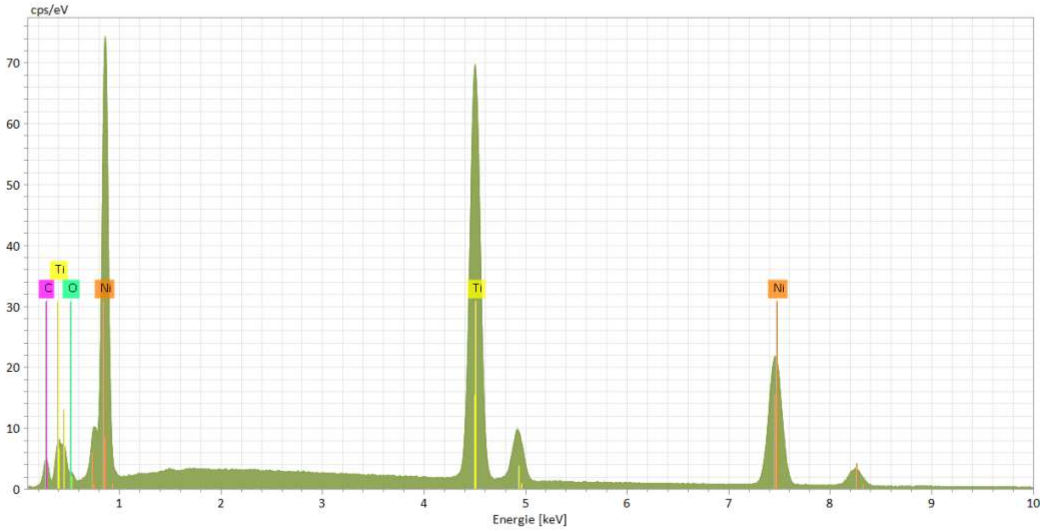

Figure 2.8 EDX result of RevoS

2.2.4 ProTaper Universal (Dentsply, Maillefer, Ballaigeus, Switzerland)

The tip diameter of the ProTaper Universal F2 file is 0.25 mm, and it has an 8% taper in the first 3 mm. Beyond this point, the taper decreases gradually. It is a conventional NiTi file. It has a convex triangular cross-section and an increasing flute design (Figure 2.9), [48]. As ProTaper Universal is no longer in production, the values related to its phase transformation behavior and elemental composition were retrieved from published literature rather than experimental analysis. Its austenite finish temperature is 11 °C [41]. The file consists of approximately 48,51 % nickel and 51,49 % titanium by atomic composition [43].

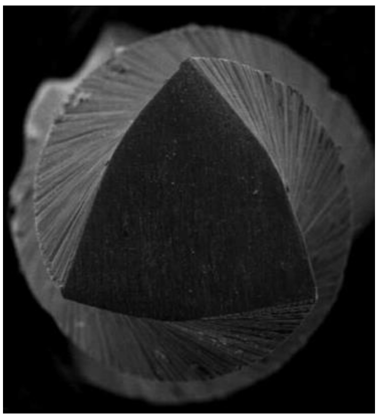

Figure 2.9 Cross section image of ProTaper Universal file [49]

2.2.5 *ProTaper Gold (Dentsply, Maillefer, Ballaigeus, Switzerland)*

ProTaper Gold instruments share the same design as ProTaper Universal, including a convex triangular cross-section and progressive taper (Figure 2.10). However, ProTaper Gold files are manufactured using proprietary heat-treated metallurgy, which provides improved flexibility compared to the original ProTaper Universal system. According to DSC analysis, its austenite finish temperature is 46,8 °C. SEM-EDX analysis revealed that the file consists of approximately 48,62 % nickel and 51,38 % titanium by atomic composition (Figure 2.11).

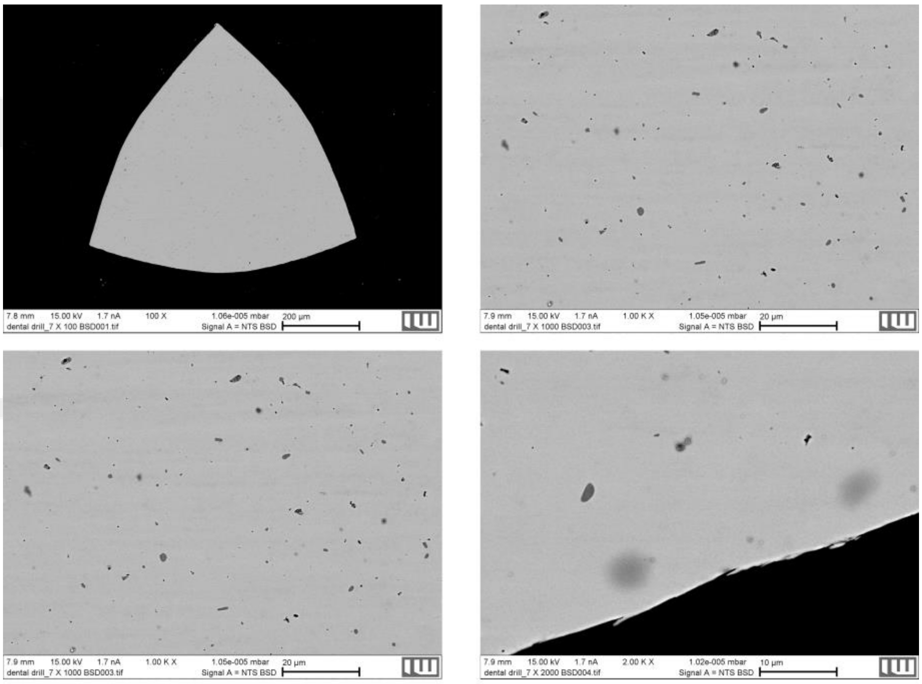

Figure 2.10 SEM images of ProTaper Gold file cross-section at increasing magnifications

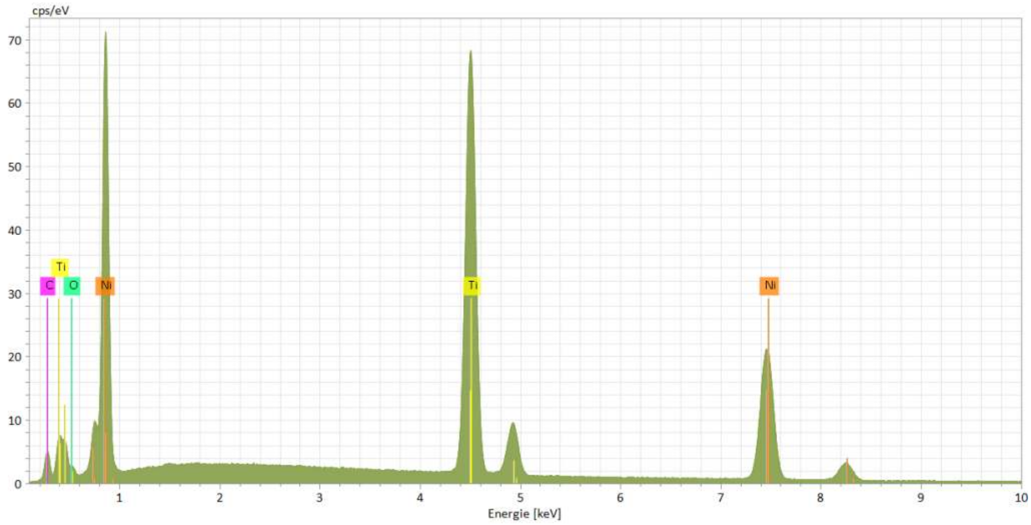

Figure 2.11 EDX result of ProTaper Gold

2.2.6 ProTaper Next (Dentsply, Maillefer, Ballaigeus, Switzerland)

ProTaper Next is one of the most widely used root canal instrumentation systems. It features a variable taper design, an off-centred rectangular cross-section, and is produced using M-Wire technology (Figure 2.12). M-Wire was developed by Sportswire LLC (Langley, OK, USA) in 2007 through a proprietary thermomechanical process aimed at producing a more flexible NiTi alloy with improved fatigue resistance [50]. The instrument has an apical diameter of 0.25 mm and a .06 taper in the first 3 mm. According to DSC analysis, its austenite finish temperature is 45,5 °C. SEM-EDX analysis revealed that the file consists of approximately 48,75 % nickel and 51,25 % titanium by atomic composition.

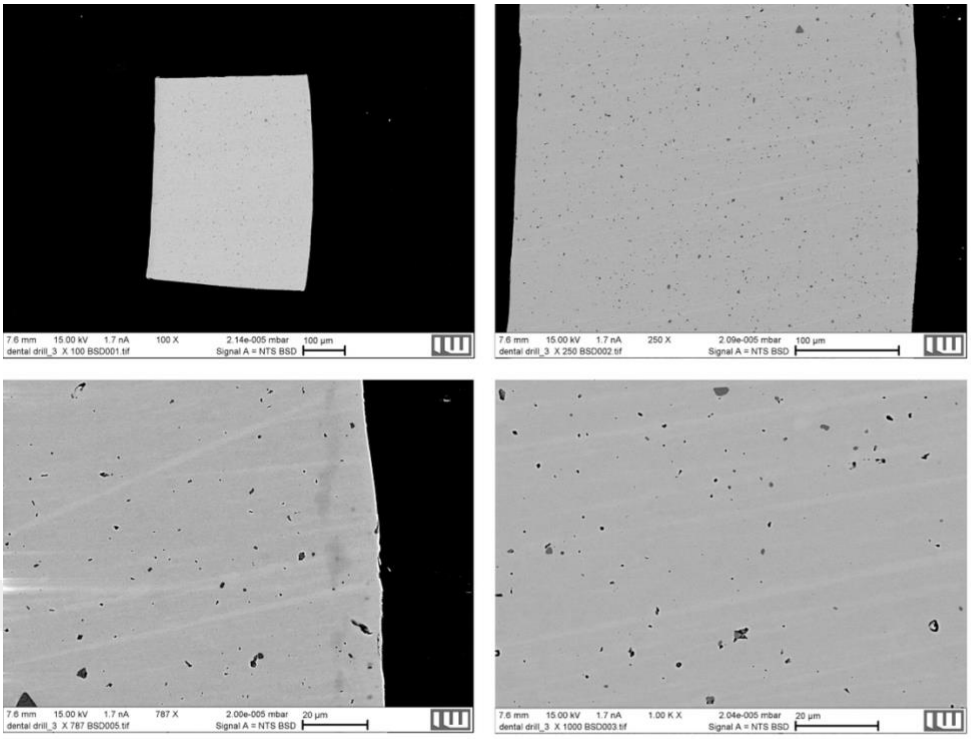

Figure 2.12 SEM images of ProTaper Next file cross-section at increasing magnifications

2.2.7 MTwo (VDW, Munich, Germany)

The Mtwo instruments have an italic "S"-shaped cross-section [51] (Figure 2.13). The system includes a file with an apical diameter of 0.25 mm and a .06 taper. It is made of conventional NiTi alloy. According to DSC analysis, its austenite finish temperature is 10,6 °C. SEM-EDX analysis revealed that the file consists of approximately 48,75 % nickel and 51,25 % titanium by atomic composition.

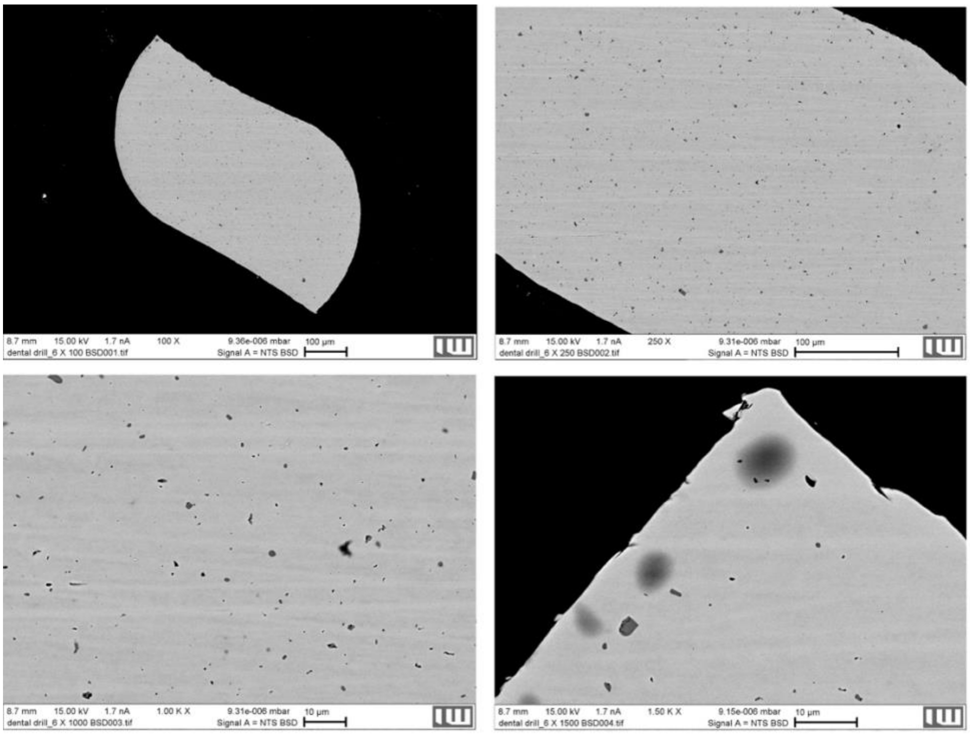

Figure 2.13 SEM images of MTwo file cross-section at increasing magnifications

2.2.8 VDW Rotate (VDW, Munich, Germany)

VDW Rotate features an S-shaped cross-section similar to that of the earlier Mtwo system, but it undergoes a proprietary heat treatment process applied by the manufacturer (Figure 2.14). The system includes a file with an apical diameter of 0.25 mm and a .06 taper. According to DSC analysis, its austenite finish temperature is 26,2 °C. SEM-EDX analysis revealed that the file consists of approximately 48,54 % nickel and 51,46 % titanium by atomic composition (Figure 2.15).

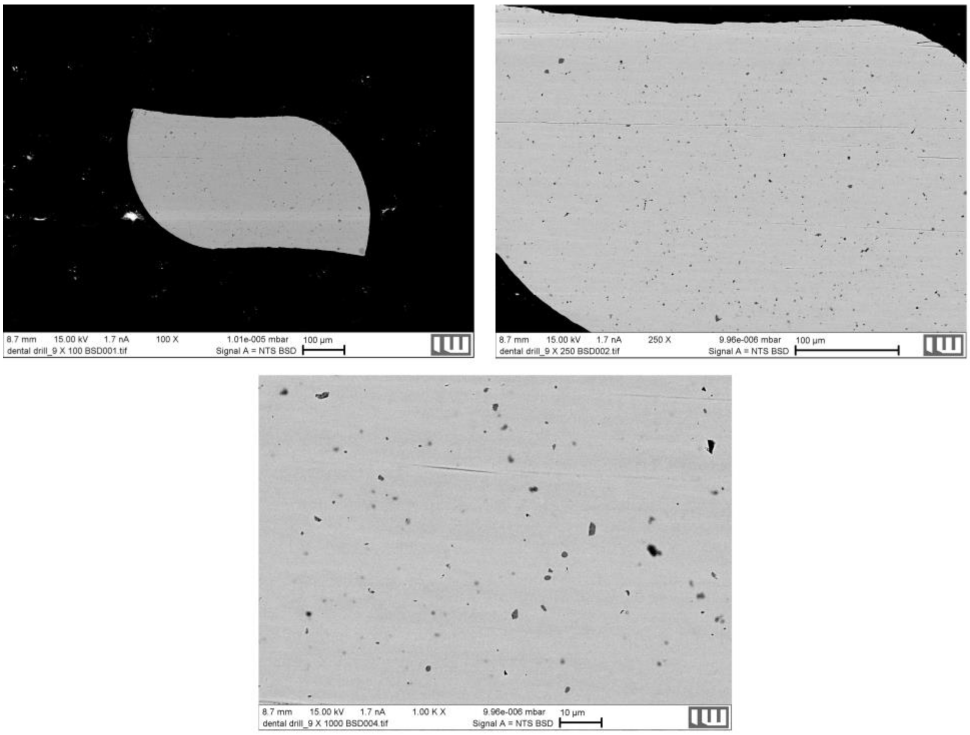

Figure 2.14 SEM images of VDW Rotate file cross-section at increasing magnifications

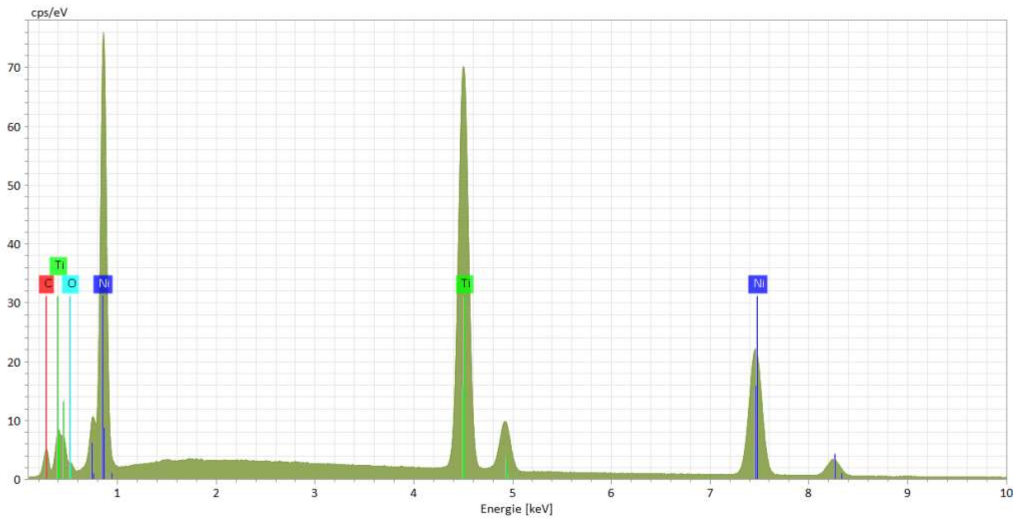

Figure 2.15 EDX result of VDW Rotate

2.2.9 Hyflex EDM (Coltene, Whaledent, Switzerland)

Controlled Memory (CM) wire, introduced in 2010, was the first thermomechanically treated NiTi alloy used in endodontics that lacks superelasticity at both room and body temperature. Unlike austenitic NiTi instruments, CM Wire files do not return to a straight shape during the preparation of curved root canals (Figure 2.16).

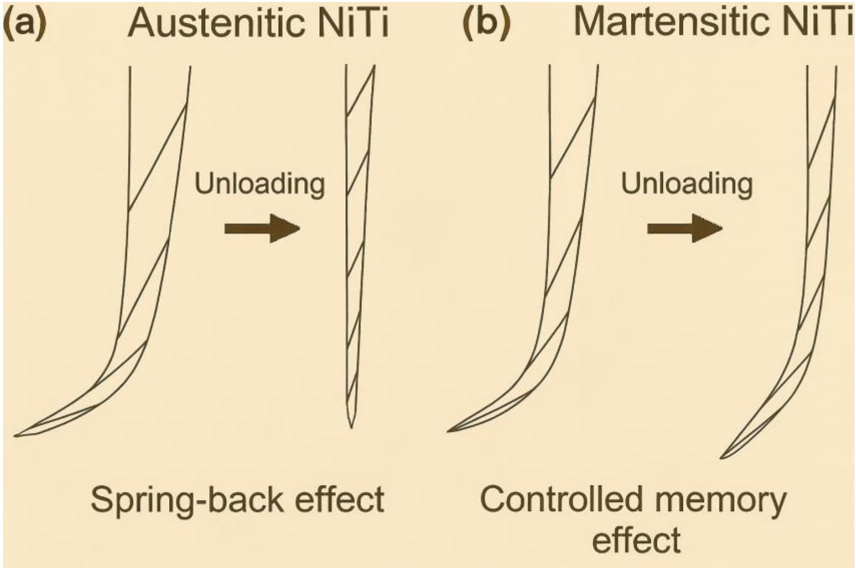

Figure 2.16 (a)Spring-back effect of austenitic NiTi alloys, (b)controlled memory effect of martensitic NiTi alloy [50]

Coltene/Whaledent later developed HyFlex EDM, a rotary NiTi system also made from CM Wire. HyFlex EDM is the first endodontic file produced using the electrical discharge machining (EDM) technique. The HyFlex EDM One File has a .08 taper in the first 4 mm of its apical region, which then gradually decreases to .04. Its design features a variable cross-section: approximately triangular near the shaft, trapezoidal in the middle, and square-shaped at the tip [50, 52] (Figure 2.18). According to DSC analysis, its austenite finish temperature is 53 °C. SEM-EDX analysis revealed that the file consists of approximately 48,53 % nickel and 51,47 % titanium by atomic composition (Figure 2.17).

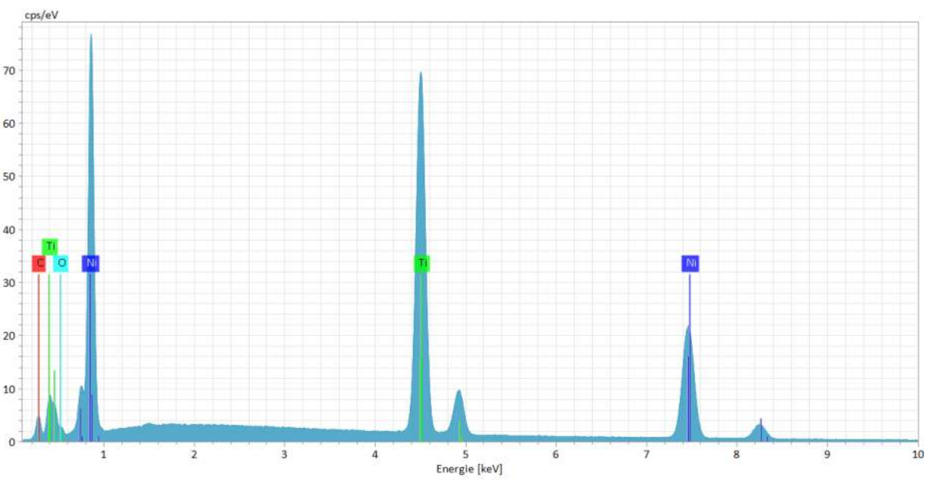

Figure 2.17 EDX result of Hyflex EDM

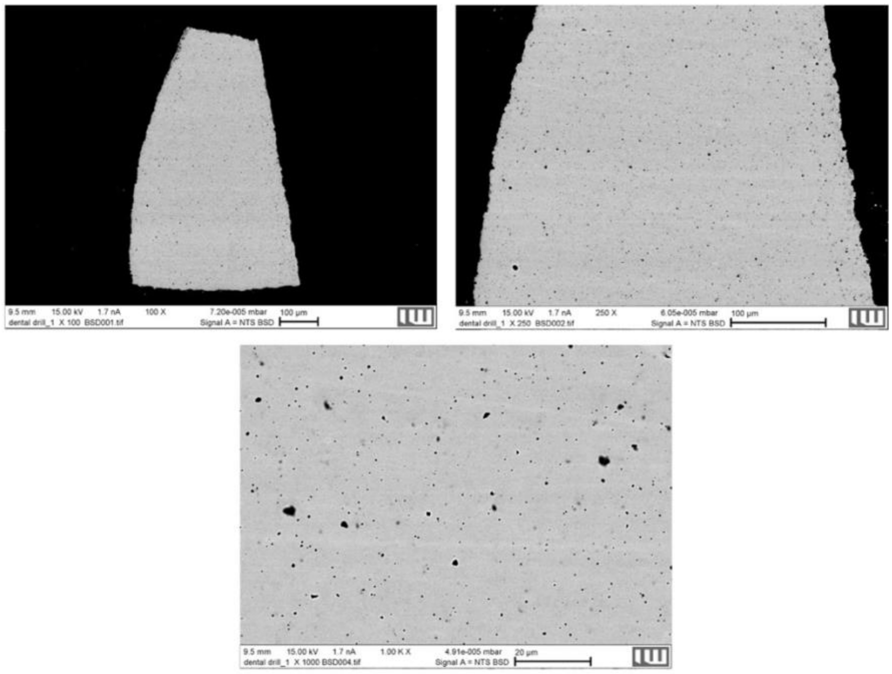

Figure 2.18 SEM images of Hyflex EDM file cross-section at increasing magnifications

The thermal and microstructural characterization of the NiTi rotary instruments revealed distinct variations in alloy behavior, which appear to be closely related to their respective manufacturing and heat treatment protocols. Differential Scanning Calorimetry analysis showed that instruments HyFlex EDM, VDW Rotate, and ProTaper Gold, ProTaper Next and OneCurve exhibited relatively high austenite finish temperatures, suggesting that these files were subjected to proprietary heat treatments designed to modify their transformation behavior. In contrast, files such as Revo-S, OneShape, MTwo, and ProTaper Universal demonstrated little to no thermal activity, consistent with a fully austenitic structure at body temperature (Figure 2.19).

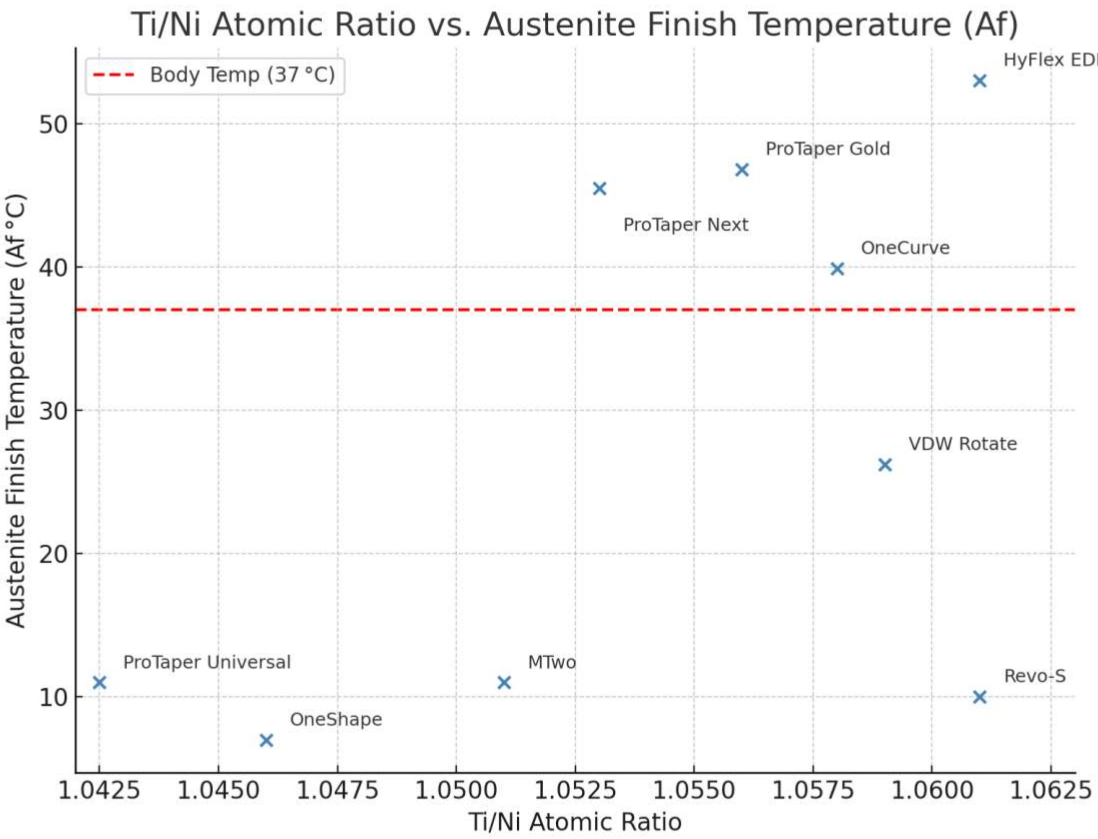

Figure 2.19 Austenite finish temperatures of selected NiTi rotary files plotted against their Ti/Ni atomic ratios. The red dashed line indicates human body temperature (37 °C).

Several instruments revealed dark-toned regions near the cutting edge, which were identified via EDX as areas of carbon enrichment likely originating from polishing residues or surface treatment processes. Additionally, Ti_2Ni intermetallic precipitates were observed within the cross-sectional matrix of multiple files. Ti_2Ni precipitates may develop in NiTi alloys with near-equiatomic composition, especially in the presence of slight titanium enrichment or under specific manufacturing conditions [53].

Chapter 3:
MACHINE LEARNING ANALYSIS

3.1 Overview

Machine learning (ML) is a branch of artificial intelligence that is widely applied in various fields. Unlike traditional computational methods, ML creates models by learning from existing data and uses these models to make predictions on new, unseen data. In other words, machines can learn from past examples and improve their performance to make decisions in unfamiliar situations. Traditional research methods often take a long time and require expensive equipment and high-quality materials. These challenges slow down the discovery and design of new materials. To solve this problem, researchers now use machine learning alongside traditional experiments, which helps reduce both time and cost significantly [54].

Depending on how learning is structured, machine learning is generally divided into three main types: supervised learning, unsupervised learning, and reinforcement learning [55]. A supervised learning algorithm is used when the desired outcome is clearly defined, but the relationships between the data elements affecting that outcome are unclear. In such cases, the goal of applying a machine learning algorithm is to uncover and learn these relationships in order to achieve the expected result [56]. The availability of labelled data is limited, and manually labelling data is often costly. This is where unsupervised learning becomes a useful alternative, and unsupervised learning identifies patterns within data that lack labels. Reinforcement learning, on the other hand, learns through interactions by choosing optimal actions that maximize reward [55, 56].

Data collection is the initial stage in both data mining and machine learning workflows. In this step, the required data is gathered in digital form from experiments, simulations, calculations, or existing databases. However, the collected data often contains noise, errors (such as out-of-range values or logically inconsistent entries), irrelevant information, or missing values. These issues can negatively affect the performance of the machine learning model. Therefore, before selecting an algorithm, such data problems must be identified and addressed. The overall quality of the dataset is typically assessed using indicators such as validity, accuracy, completeness, consistency, and uniformity. In many cases, this data cleaning process is considered part of data preprocessing [54].

The training and testing process is the most crucial element influencing the success of a machine learning model. A well-structured training process enhances the overall performance of the system. Typically, researchers split datasets into training and testing subsets. The proportion of data allocated to training and testing greatly affects model accuracy. When there is a strong correlation between input features and the target variable, a 50%–50% split can be used, half of the data for training and the other half for testing. However, to avoid poor performance, increasing the training ratio is often preferred. The optimal training-testing ratio depends on the nature of the dataset. Using less than 50% of the data for training is generally discouraged, as it may negatively impact test results. Once the model is trained with the training data, it is also evaluated on that same data to assess how well the model has learned [57].

Before applying a machine learning model, it is essential to consider the risks of overfitting and underfitting. These problems mainly result from bias and variance. Bias refers to the model's inability to learn from the data properly, leading to inaccurate predictions, and this is known as underfitting. In such cases, the model cannot capture the complexity of the data. Increasing the amount of data or simplifying the model can help reduce underfitting. On the other hand, high variance means the model is overly sensitive to the training data, which can cause overfitting. An overfitted model performs well on training data but poorly on new, unseen data. Therefore, balancing bias and variance is essential for building a reliable model [54].

In light of the importance of proper model training and data splitting strategies, various machine learning algorithms were employed in this study to evaluate their predictive capabilities. These models were selected based on their suitability for small datasets, ability to handle multivariate features, and generalization performance. Accordingly, the machine learning algorithms used in this study are briefly described below.

The random forest algorithm, introduced by L. Breiman in 2001, has proven to be a highly effective method for both classification and regression tasks. It works by combining multiple randomized decision trees and averaging their predictions. This approach performs particularly well in situations where the number of features is much greater than the number of data samples. In addition, it is flexible enough to handle large-scale problems, can be adapted to various specific learning tasks, and provides information about the importance of each variable [58].

Gradient Boosted Decision Trees (GBDT) are popular machine learning models due to their accuracy, speed, and ease of understanding. GBDT works by building a series of decision trees, where each tree tries to correct the mistakes made by the previous ones. The final result is the sum of all tree predictions. In most versions of GBDT, each tree gives only one output value. If there are multiple output variables, the model creates separate trees for each one. However, this method does not consider the relationships between the outputs, which can lead to repeated or unnecessary tree structures. This happens because each leaf in a tree can only produce a single output [59].

Linear regression is one of the simplest methods used for regression analysis. It is also one of the most widely used techniques in predictive modelling. The main goal of linear regression is to find a straight line that best fits the scatter plot of the data. In practice, many possible lines are tested, and the one that most closely matches the data points, by minimizing the error, is selected as the best-fitting line [60, 61].

The K-Nearest Neighbors (KNN) algorithm is a non-parametric method, meaning it does not assume any specific underlying data distribution. It is a supervised learning approach known for its simplicity and effectiveness. KNN uses a labeled training dataset in which data points belong to known classes, allowing the model to predict the class of new, unlabeled data based on the closest training examples [62].

XGBoost, which stands for Extreme Gradient Boosting, is an advanced ensemble learning algorithm based on Gradient Boosted Decision Trees (GBDT). The core idea behind boosting is that combining multiple weak decision trees can result in a much stronger predictive model. While a single tree may not perform well on its own, the overall accuracy improves significantly when many trees are combined. XGBoost applies this principle efficiently and is known for its speed, flexibility, and high prediction performance in both classification and regression tasks [63, 64]

3.2 Data Mining

A preliminary search of the PubMed database using the keywords “cyclic fatigue” and “endodontics” yielded a large number of publications. Since the primary aim of this study was to determine the optimum NiTi composition, and because parameters such as apical diameter, taper, and movement kinematics may influence cyclic fatigue resistance, only files working with continuous rotation, with an apical diameter of 0.25 mm, and a 6% taper were included in the study.

After evaluating the commercially available systems that meet these criteria, the following file systems were selected for inclusion:

- ProTaper Next
- ProTaper Universal
- ProTaper Gold
- MTwo
- VDW Rotate
- OneShape
- OneCurve
- Revo-S
- HyFlex EDM

Following the selection of eligible instruments, an English-limited PubMed database search was performed. The searched keywords included “ProTaper Universal” or “ProTaper Gold” or “ProTaper Next” or “Mtwo” or “VDW Rotate” or “OneShape” or “OneCurve” or “RevoS” or “Hyflex EDM” and “cyclic fatigue”.

This search resulted in a total of 233 articles. Review papers that did not fit with the aim of the current study were excluded. The remaining articles were then re-evaluated according to specific inclusion criteria.

Some of the aforementioned file systems also include instruments with sizes other than 25.06. Studies evaluating other file sizes were excluded from the analysis. Furthermore, the following exclusion criteria were applied:

- Studies that did not report the NCF
- Use of a double-curved or S-shaped experimental setup
- Absence of a clearly defined curvature angle and radius
- Use of a combined fracture testing model (cyclic and torsional fatigue together)
- Experiments conducted at body temperature
- Evaluation of previously used instruments
- Contact of files with irrigating solutions or assessment of fatigue resistance after sterilization

Studies that met any of these conditions were excluded from the dataset. According to the criteria described above, 89 studies were identified as relevant. From these studies, a total of 183 data instances were extracted. The input parameters used in this study were then determined. Experimental conditions were represented by two parameters: Curvature radius and angle. Material-related features were defined as follows:

- A_f temperature
- Nickel content (at%)
- Titanium content (at%)
- Electronegativity
- Valence electron number
- Atomic mass
- Atomic radius

The A_f temperature and the atomic percentages of Ni and Ti were not available in the literature for all included instruments. Therefore, these values were experimentally obtained through DSC and SEM-EDX analyses (Chapter 2). It is well known that heat treatment has a significant impact on the cyclic fatigue resistance of NiTi instruments. Although the specific heat treatment protocols could have been valuable input data, these procedures are considered trade secrets by the manufacturers; therefore, detailed information is not accessible. For this reason, the presence of heat treatment was included in the dataset as a binary variable (0 = no heat treatment, 1 = heat treatment applied) (Table 3.1).

Table 3.1 Description of Input and Output Features Used in the Dataset before preprocessing

Feature Name	Unit	Description	Source	Data Type
Curvature Radius	mm	Radius of curvature in the cyclic fatigue test setup	Literature	Numerical
Curvature Angle	Degrees (°)	Angle of curvature in the test setup	Literature	Numerical
Electronegativity	Pauling Scale	Electronegativity of the alloy based on weighted atomic contribution	Calculated	Numerical
Valence Electron No.	-	Total valence electron number (composition-based)	Calculated	Numerical
Atomic Radius	pm	Average atomic radius of elements in the alloy	Calculated	Numerical
Atomic Mass	g/mol	Average atomic mass of the alloy components	Calculated	Numerical
Af Temperature	°C	Austenite finish temperature	DSC analysis	Numerical
Ni Content	Atomic %	Atomic percentage of Nickel in the alloy	SEM-EDX analysis	Numerical
Ti Content	Atomic %	Atomic percentage of Titanium in the alloy	SEM-EDX analysis	Numerical
Heat Treatment Applied	Binary (0 = No, 1 = Yes)	Indicates whether the file underwent heat treatment	Manufacturer / Literature	Categorical
NCF	-	Number of Cycles to Failure (output)	Literature	Numerical

3.3 Dataset Preparation

During the initial preprocessing stage, it was found that the electronegativity remained constant across all samples. Since features with no variation do not contribute to the learning process and may introduce noise, this parameter was removed from the input feature set. Therefore, the final model was trained using the remaining variables, which were more informative and effective in capturing the patterns relevant to the target property.

To assess the potential relationships between input variables and to identify possible redundancy or multicollinearity, a Pearson correlation matrix was constructed. The correlation heatmap provides valuable insight into the linear dependencies among the variables. As shown in Figure 3.1, austenite finish temperature exhibits the highest positive correlation with NCF ($r = 0.32$), indicating that variations in A_f are moderately aligned with changes in the NCF. Conversely, angle shows a negative correlation with NCF ($r = -0.29$), suggesting a mild inverse relationship. Most other features, including Ni, Ti, atomic mass, and Valence electron number, exhibit weak correlations with NCF, with absolute correlation coefficients of around 0.28 or less, implying that these variables may contribute more subtle or nonlinear effects to the prediction task.

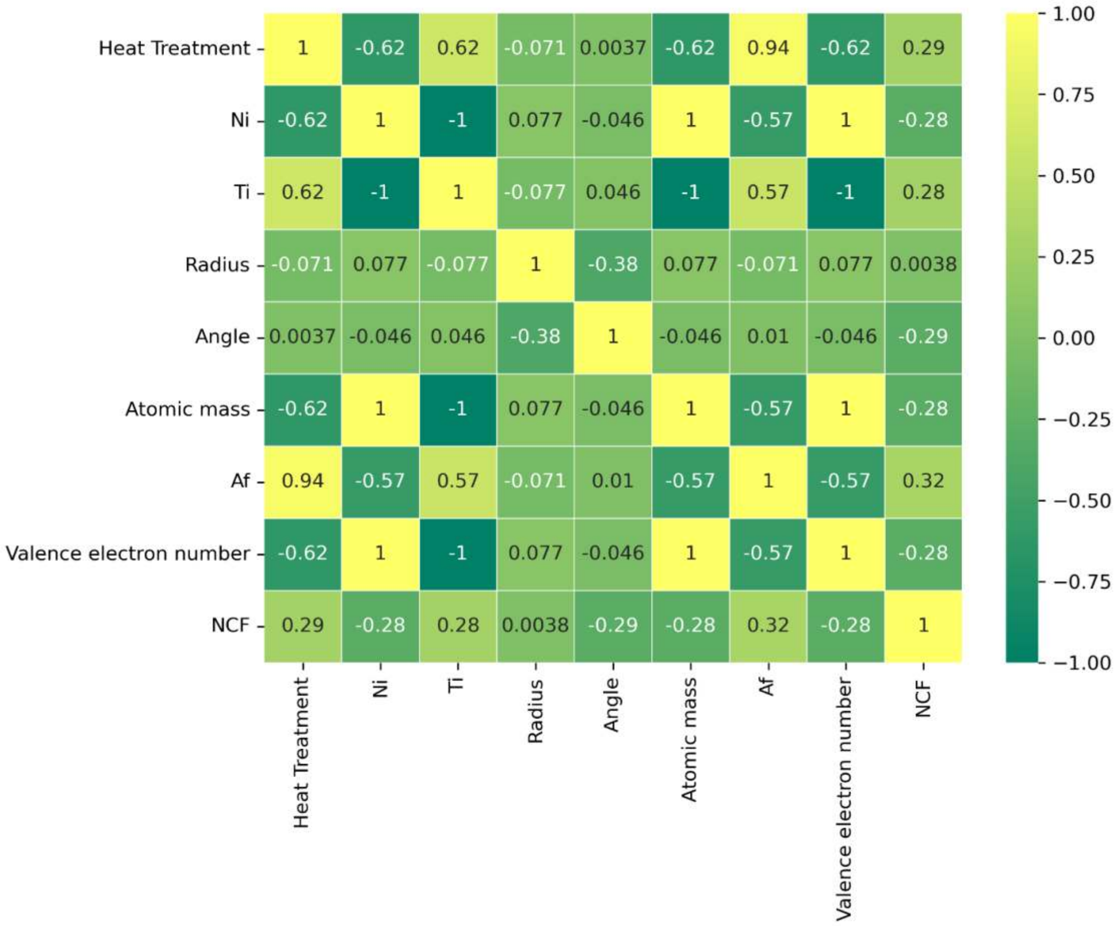

Figure 3.1 Pearson correlation heatmap illustrating the linear relationships among input features and the target variable (NCF).

Additionally, high intercorrelations are observed among some input features. For instance, Ni, Ti, Atomic mass, and Valence electron number are perfectly correlated ($r = \pm 1$), indicating potential redundancy in the dataset. Similarly, heat treatment is strongly correlated with A_f ($r = 0.94$), suggesting that the heat treatment condition largely governs the austenite finish temperature. These correlations suggest that dimensionality reduction techniques or feature selection methods may be beneficial for eliminating collinear features and enhancing model performance. Overall, the correlation analysis supports the relevance of A_f and Angle in predicting NCF, while also highlighting areas where feature redundancy should be addressed before finalizing the model input set.

As explained, it was observed that certain input variables exhibited perfect linear correlation ($r = \pm 1$). Specifically, Ti showed a correlation of -1 with Ni, while both atomic mass and valence electron number had a perfect positive correlation ($r = 1$) with Ni. Since these features are linearly dependent, retaining all of them would introduce redundancy into the model, increasing the risk of overfitting. Therefore, Ti, atomic mass, and valence electron number were removed from the input feature set. This step helped simplify the model without sacrificing meaningful variance in the data, while also enhancing generalizability and interpretability (Figure 3.2).

Figure 3.2 Correlation heatmap for the selected input variables after feature elimination.

To improve the quality and reliability of the machine learning model, an outlier detection and removal process was applied to the dataset, particularly focusing on the output variable, NCF. The presence of extreme outliers in the original dataset led to a highly skewed distribution, as observed in the Original Output Distribution plot (Figure 3.3). A significant concentration of data points was observed at lower NCF values, while a small number of extreme values extended beyond 12,000, potentially introducing bias and reducing the model's generalizability.

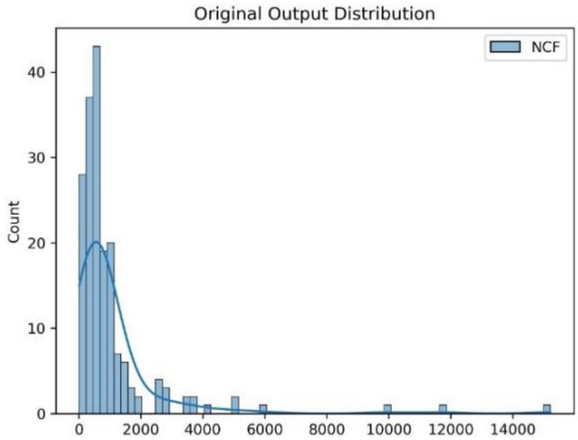

Figure 3.3 Original Output Distribution of NCF.

To address this issue, unsupervised outlier detection was performed by varying the contamination level, which represents the proportion of data suspected to be outliers. As shown in the Effect of Contamination Level on R² Score plot (Figure 3.4), cross-validated R² scores were calculated for different contamination thresholds. Initially, the R² score was strongly negative due to the high impact of outliers. However, as the contamination level increased (i.e., more outliers were removed), the cross-validated R² score improved, reaching its optimal value around a contamination level of 0.15. This improvement indicates that removing highly deviant data points led to a model that better captured the underlying patterns in the data.

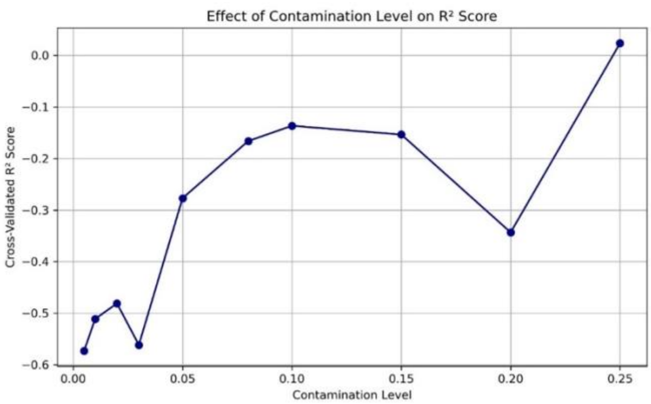

Figure 3.4 Effect of Contamination Level on R² Score

The effectiveness of outlier removal is further visualized in the Cleaned Output Distribution plot (Figure 3.5), where the NCF distribution is noticeably more balanced and approximately unimodal. Compared to the original skewed distribution, the cleaned dataset exhibits a more uniform spread, which enhances model performance and stability by reducing the influence of extreme values.

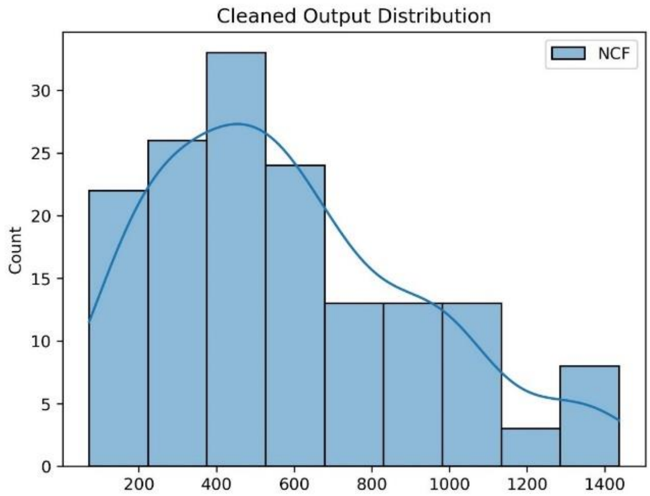

Figure 3.5 Cleaned Output Distribution of NCF

Overall, the combined analysis supports the decision to remove approximately 15% of the most extreme data points from the dataset. This preprocessing step was essential for mitigating the adverse effects of outliers and improving the model's predictive accuracy and robustness.

3.3.1 Feature Distribution Analysis Using Violin Plots

The violin plots presented in the figure provide a visual representation of the distribution and variability of each input feature, both before and after feature selection. These plots combine a box plot with a kernel density estimate (KDE), enabling the visualization of data concentration, spread, skewness, and potential outliers for each feature.

In Figure 3.6, which corresponds to the original dataset before feature selection, all initial features, including Ni, Ti, Atomic mass, and Valence electron number, are shown. Several variables, particularly Radius and NCF, exhibit wide distributions with long tails, indicating the presence of extreme values or skewed distributions. Additionally, features such as Ti, Atomic mass, and Valence electron number show remarkably similar distributions, which is consistent with the earlier correlation analysis indicating high redundancy (r = ±1) among them. The inclusion of these redundant features not only introduces multicollinearity but can also lead to overfitting and reduced model generalizability.

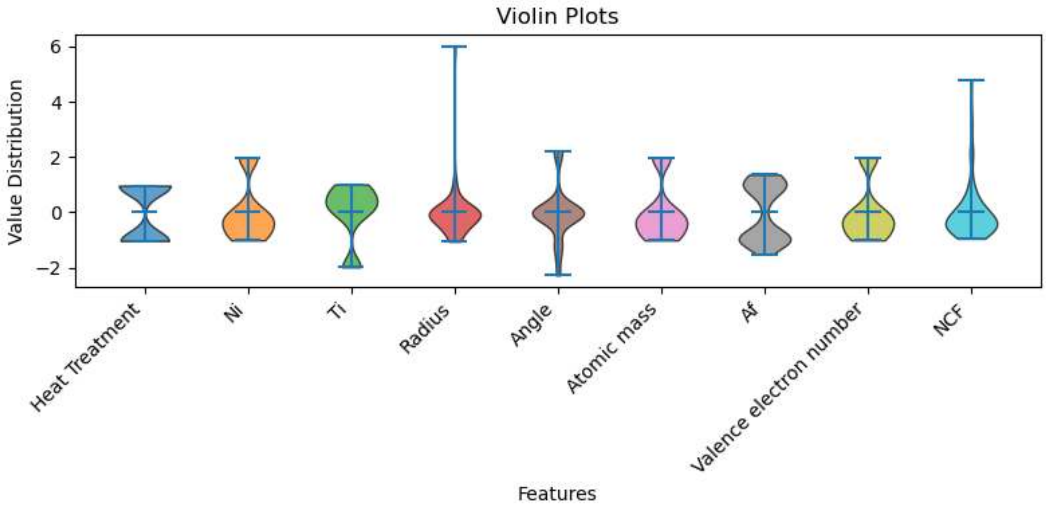

Figure 3.6 Violin plots of the input features before feature selection

In contrast, Figure 3.7 illustrates the distributions after redundant and highly correlated features were removed, retaining only the most informative and independent variables. Notably, Ti, Atomic mass, and Valence electron number have been eliminated, resulting in a more compact and diverse set of input features. The resulting distributions remain well-structured, with Radius, A_f, and Angle maintaining adequate variance, ensuring that the retained features still cover a broad and informative range of values for modelling. The exclusion of multicollinear features reduces noise and complexity, allowing the machine learning model to focus on truly predictive information.

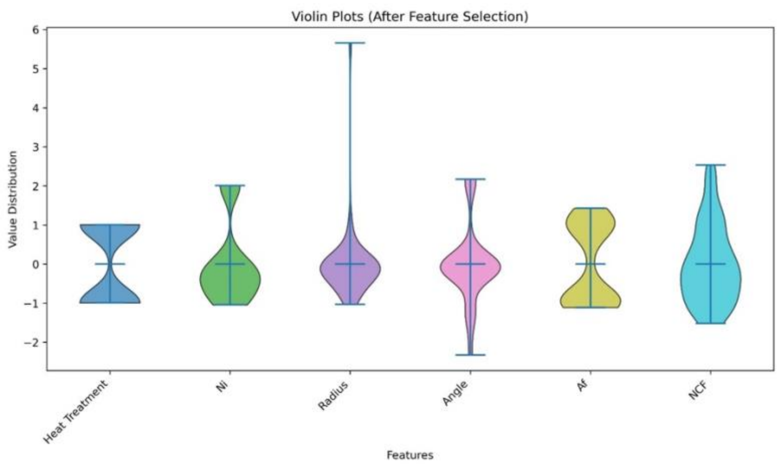

Figure 3.7 Violin plots of the input features after feature selection

Overall, the comparison between the two plots highlights the impact of careful feature selection on data quality. By eliminating redundant variables, the feature space becomes more efficient, improving model interpretability and reducing the risk of overfitting, ultimately leading to more accurate and stable predictions of the target property, NCF.

As observed, the inter-feature correlations are relatively high, whereas the correlations between the input features and the target variable (NCF) are generally low. This imbalance negatively affects the accuracy of predictive models, as it suggests that the input variables are more closely related to one another than to the target, potentially leading to redundant information and model instability.

Moreover, the violin plots demonstrate that the distributions of the features are not normal. These plots visualize the 25th percentile, median, and 75th percentile, allowing us to assess the skewness and spread of the data. In most cases, the data distributions are not centred around the median, further confirming the lack of normality or uniformity. Such irregular and skewed distributions can significantly impact the performance of machine learning models, particularly when predicting the NCF value, as many models rely on certain assumptions regarding data distribution to achieve optimal performance

3.4 Machine Learning Model

In machine learning, effectively managing input features is essential to maintaining generalization and reliability. High correlation among features can introduce multicollinearity, which undermines model performance by inflating prediction errors and decreasing robustness. To mitigate this, feature selection is necessary to identify and remove redundant features. Therefore, in this study, to effectively manage input variables and enhance model accuracy, two different methods were employed to assess and select features: Pearson Correlation Coefficient (PCC) and Random Forests (RF).

To evaluate the effectiveness of these feature selection techniques in improving predictive performance, we trained multiple models using each feature selection method. By selecting the best-performing feature sets for each model, we aimed to determine the most effective combination of model and feature selection approach. These optimized models were then compared, providing deeper insights into how different models are influenced by various feature selection techniques. This analysis enabled a more nuanced understanding of their impact on prediction accuracy, helping to identify the most suitable approach for this study.

To develop the predictive model, various machine learning algorithms were employed, including Random Forest, Gradient Boosted Decision Trees, Support Vector Regression, Linear Regression, K-Nearest Neighbors, and Extreme Gradient Boosting. To make the ranges and distributions of all features consistent and comparable, thereby boosting training performance and efficiency, standardization was applied by scaling all features to a zero mean and unit variance. Model performance was rigorously evaluated using a 10-fold cross-validation (CV) approach.

To identify the most suitable predictive model, the input features were ranked based on their importance as determined by feature selection methods, RF and PCC. The models were then trained incrementally using these ranked features. For each configuration, performance metrics including the coefficient of determination (R^2), root mean squared error (RMSE), and mean absolute error (MAE) were calculated. The results are summarized in Tables 3.2 to 3.6, which provide a comparative overview of model performance under different feature combinations.

3.4.1 Model Evaluation Based on PCC Feature Selection

To evaluate the impact of feature selection on model performance, a stepwise feature inclusion approach was employed using the Pearson Correlation Coefficient (PCC) as the selection criterion. Features were ranked according to their correlation with the target variable (NCF), and models were trained by incrementally adding the top-ranked features. Performance was assessed using three key metrics: R^2 score, Root Mean Squared Error (RMSE), and Mean Absolute Error (MAE) on both training and testing datasets. The models considered included Random Forest (RF), Gradient Boosting Decision Tree (GBDT), Support Vector Regression (SVR), Linear Regression (LR), K-Nearest Neighbors (KNN), and Extreme Gradient Boosting (XGB).

Figure 3.8 shows the ordered importances of all non-elemental features according to the PCC method. As shown, the most important parameters are ranked by their importance, with delta Ni and A_f emerging as the most significant factors in PCC feature selection method.

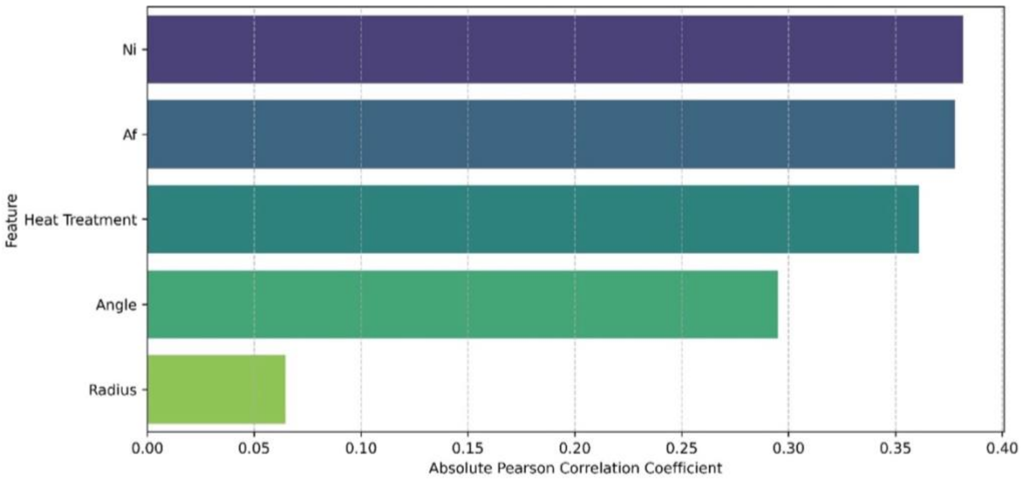

Figure 3.8 Feature importance ranking based on the absolute Pearson correlation coefficient with NCF.

Top 1 Feature: [Ni]

The initial model trained using only the top feature - Ni - yielded relatively poor performance across all metrics, with low R^2 scores (e.g., 0.083 for test in RF) and high RMSE values. Despite the weak predictive power, SVR slightly outperformed other models, particularly on the test set (Table 3.2).

Table 3.2 PCC: Selecting top 1 feature – [Ni]

	RF	**GBDT**	**SVR**	**LR**	**KNN**	**XGB**
Train RMSE	0.912	0.912	0.914	0.912	0.968	0.913
Test RMSE	0.910	0.911	0.909	0.911	1.002	0.913
Train MAE	0.727	0.727	0.728	0.727	0.779	0.729
Test MAE	0.740	0.741	0.744	0.741	0.821	0.743
Train R2	0.168	0.168	0.164	0.168	0.060	0.165
Test R2	0.083	0.083	0.094	0.082	-0.115	0.085

Best Model: SVR

Top 2 Features: [Ni, A_f]

When the second feature, A_f content, was added, all models showed notable improvement. Test R^2 scores increased (e.g., from 0.083 to 0.233 in SVR), and RMSE and MAE values decreased accordingly. This indicated that A_f had a stronger influence on NCF and improved generalization (Table 3.3).

Table 3.3 PCC: Selecting top 2 features - [Ni, Af]

	RF	GBDT	SVR	LR	KNN	XGB
Train RMSE	0.825	0.824	0.847	0.895	0.839	0.830
Test RMSE	0.853	0.864	0.838	0.898	0.883	0.856
Train MAE	0.623	0.625	0.640	0.694	0.648	0.636
Test MAE	0.663	0.675	0.652	0.713	0.702	0.675
Train R2	0.318	0.319	0.281	0.199	0.294	0.311
Test R2	0.182	0.161	0.233	0.114	0.127	0.185

Best Model: SVR

Top 3 Features: [Ni, A_f, Heat Treatment]

Introducing the third feature, heat treatment, slightly enhanced training metrics, but had a limited effect on test performance. The marginal gains suggest that heat treatment contributes moderately to the model but may not generalize well across unseen data (Table 3.4).

Table 3.4 PCC: Selecting top 3 features - [Ni, Af, Heat Treatment]

	RF	GBDT	SVR	KNN	XGB
Train RMSE	0.825	0.824	0.833	0.848	0.829
Test RMSE	0.859	0.866	0.846	0.892	0.860
Train MAE	0.625	0.624	0.629	0.660	0.636
Test MAE	0.671	0.677	0.661	0.705	0.679
Train R2	0.318	0.319	0.305	0.279	0.311
Test R2	0.170	0.158	0.209	0.111	0.178

Best Model: SVR

Top 4 Features: [Ni, Af, Heat Treatment, Angle]

The addition of Angle as the fourth feature resulted in more consistent performance improvements. Notably, SVR again achieved the highest test R^2 score (0.321), with the lowest RMSE (0.785) and MAE (0.609) among all models. These results confirm the model's robustness when incorporating moderately correlated geometric features like angle (Table 3.5).

Table 3.5 PCC: Selecting top 4 features - [Ni, Af, Heat Treatment, Angle]

	RF	GBDT	SVR	LR	KNN	XGB
Train RMSE	0.729	0.662	0.728	0.832	0.759	0.724
Test RMSE	0.842	0.885	0.785	0.851	0.814	0.840
Train MAE	0.564	0.500	0.526	0.657	0.605	0.565
Test MAE	0.666	0.682	0.609	0.686	0.664	0.665
Train R2	0.468	0.561	0.470	0.307	0.422	0.475
Test R2	0.218	0.122	0.321	0.208	0.271	0.228

Best Model: SVR

Top 5 Features: [Ni, A_f, Heat Treatment, Angle, Radius]

Upon including the fifth feature, Radius, the performance trend plateaued or slightly declined for some models. Although KNN emerged as the best model in this setup (Test $R^2 = 0.303$), the differences across models became less significant (Table 3.6).

Table 3.6 PCC: Selecting top 5 features - [Heat Treatment, Ni, Af, Angle, Radius]

	RF	GBDT	SVR	LR	KNN	XGB
Train RMSE	0.664	0.593	0.704	0.830	0.743	0.697
Test RMSE	0.847	0.885	0.802	0.878	0.794	0.843
Train MAE	0.518	0.450	0.551	0.655	0.587	0.548
Test MAE	0.675	0.696	0.654	0.702	0.640	0.677
Train R2	0.559	0.648	0.503	0.310	0.447	0.513
Test R2	0.206	0.126	0.296	0.150	0.303	0.221

Best Model: KNN

Overall, the results suggest that optimal model performance using PCC-based feature selection is achieved with the top 4–5 features. SVR consistently performed best across different stages, especially when using Heat Treatment, Ni, A_f, and Angle as inputs. However, KNN showed competitive performance when more features were added.

3.4.2 Model Evaluation Based on Random Forest (RF) Feature Selection

To further assess the predictive performance of various machine learning algorithms, feature selection was conducted using the Random Forest (RF) importance-based ranking. The top features were incrementally added in the order of importance, and model performance was evaluated using R^2, RMSE, and MAE for both training and testing datasets. The main objective was to identify the optimal combination of features and the most robust learning algorithm for predicting the NCF.

Figure 3.9 shows the ordered importances of all non-elemental features according to the RF method. As shown, the most important parameters are ranked by their importance, with delta Ni and Angle emerging as the most significant factors.

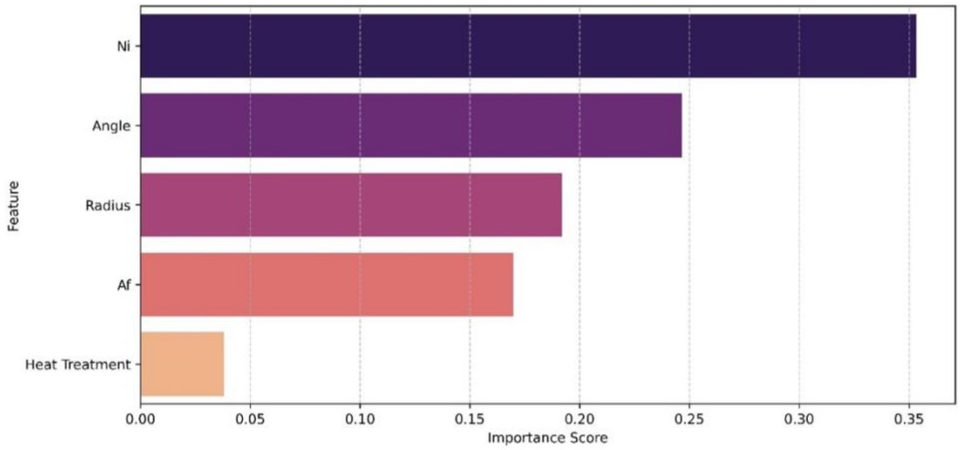

Figure 3.9 Feature importance ranking based on the RF with NCF.

Top 1 Feature: [Ni]

With only Ni as the input feature, the models performed moderately. Among all methods, XGB (Extreme Gradient Boosting) achieved the best generalization with a test R^2 of 0.189, outperforming other algorithms in both RMSE and MAE. This suggests that Ni, as a standalone feature, carries meaningful information for predicting NCF, yet it lacks sufficient explanatory power on its own (Table 3.7).

Table 3.7 RF: Selecting Top 1 Feature - [Ni]

	RF	GBDT	SVR	LR	KNN	XGB
Train RMSE	0.826	0.825	0.872	0.922	0.835	0.830
Test RMSE	0.851	0.860	0.882	0.915	0.872	0.854
Train MAE	0.623	0.625	0.654	0.721	0.645	0.636
Test MAE	0.662	0.671	0.688	0.729	0.691	0.672
Train R2	0.317	0.319	0.239	0.149	0.301	0.310
Test R2	0.185	0.170	0.141	0.089	0.146	0.189

Best Model: XGB

Top 2 Features: [Ni, Angle]

Adding Angle led to an observable improvement in training performance, especially for RF and GBDT, with RF achieving Train R^2 = 0.452 and Test R^2 = 0.232. Although test metrics slightly improved, the gap between train and test results indicates potential overfitting in GBDT. RF remained the best performer at this stage, likely benefiting from its internal feature bagging and robust handling of interactions (Table 3.8)

Table 3.8 RF: Selecting Top 2 Features - [Ni, Angle]

	RF	GBDT	SVR	LR	KNN	XGB
Train RMSE	0.740	0.683	0.865	0.860	0.799	0.731
Test RMSE	0.834	0.885	0.854	0.856	0.842	0.839
Train MAE	0.567	0.514	0.677	0.681	0.624	0.565
Test MAE	0.652	0.678	0.686	0.691	0.675	0.655
Train R2	0.452	0.532	0.250	0.259	0.360	0.465
Test R2	0.232	0.126	0.214	0.202	0.209	0.230

Best Model: RF

Top 3 Features: [Ni, Angle, Radius]

Introducing Radius as the third feature led to more consistent performance across models. SVR achieved the best balance with Test R^2 = 0.225, while maintaining moderate RMSE and MAE. The improvements in SVR and RF suggest that geometric factors, such as angle and radius, add complementary value to compositional features, thereby enhancing the model's ability to capture NCF variability (Table 3.9).

Table 3.9 RF: Selecting Top 3 Features - [Ni, Angle, Radius]

	RF	GBDT	SVR	LR	KNN	XGB
Train RMSE	0.729	0.620	0.782	0.858	0.808	0.711
Test RMSE	0.841	0.864	0.843	0.885	0.862	0.845
Train MAE	0.566	0.467	0.594	0.680	0.621	0.553
Test MAE	0.668	0.678	0.664	0.709	0.673	0.673
Train R2	0.467	0.615	0.388	0.263	0.346	0.494
Test R2	0.220	0.170	0.225	0.138	0.175	0.220

Best Model: SVR

Top 4 Features: [Ni, Angle, Radius, A_f]

With the inclusion of Af, the models showed slight gains in both training and testing metrics. The KNN model stood out with Test R^2 = 0.283, indicating its adaptability to localized patterns introduced by A_f. This shows that Af, despite being weakly correlated with NCF individually, provides useful contextual information when combined with other features (Table 3.10).

Table 3.10 RF: Selecting Top 4 Features - [Ni, Angle, Radius, Af]

	RF	GBDT	SVR	LR	KNN	XGB
Train RMSE	0.721	0.592	0.715	0.836	0.748	0.697
Test RMSE	0.850	0.883	0.815	0.877	0.807	0.843
Train MAE	0.566	0.450	0.557	0.659	0.589	0.549
Test MAE	0.682	0.697	0.662	0.703	0.647	0.677
Train R2	0.479	0.648	0.488	0.300	0.439	0.513
Test R2	0.205	0.129	0.276	0.154	0.283	0.222

Best Model: KNN

Top 5 Features: [Ni, Angle, Radius, A_f, Heat Treatment]

The final step incorporated Heat Treatment as the fifth feature. While training scores continued to improve, test performance reached a plateau across all models. KNN again emerged as the best model, achieving Test R^2 = 0.303 and the lowest test RMSE (0.794). These results highlight that the top five features, particularly a combination of compositional, thermal, and geometric parameters, collectively capture the essential variance needed for accurate prediction. (Table 3.11).

Table 3.11 RF: Selecting Top 5 Features - [Ni, Angle, Radius, A_f, Heat Treatment]

	RF	GBDT	SVR	LR	KNN	XGB
Train RMSE	0.721	0.593	0.704	0.830	0.743	0.697
Test RMSE	0.849	0.885	0.802	0.878	0.794	0.843
Train MAE	0.564	0.450	0.551	0.655	0.587	0.548
Test MAE	0.680	0.697	0.654	0.702	0.640	0.677
Train R2	0.480	0.648	0.503	0.310	0.447	0.513
Test R2	0.206	0.124	0.296	0.150	0.303	0.221

Best Model: KNN

The RF-based feature selection process revealed that a combination of Ni, Angle, Radius, A_f, and Heat Treatment provides the best performance in predicting NCF. Although models like RF and XGB performed well in early stages, KNN and SVR demonstrated superior test set generalization as more features were added. The results emphasize the importance of multi-domain feature integration and validate the effectiveness of RF feature selection in identifying meaningful inputs for model training.

Table 3.12 summarizes the highest test R^2 scores obtained at each feature count (Top 1 to Top 5) using Pearson Correlation Coefficient (PCC) and Random Forest (RF) based feature selection. It also highlights the corresponding best-performing machine learning models. Results reveal that SVR dominated performance in the early PCC stages, while KNN achieved the highest generalization for both methods when five features were used

Table 3.12 Comparison of Best-Performing Models and R^2 Scores under PCC and RF Feature Selection Strategies

Number of Features	PCC: Best R^2	Best Model-PCC	RF: Best R^2	Best Model-RF
Top 1	0.0938	SVR	0.1890	XGB
Top 2	0.2326	SVR	0.2322	RF
Top 3	0.2093	SVR	0.2248	SVR
Top 4	0.2407	SVR	0.2834	KNN
Top 5	0.3032	KNN	0.3032	KNN

Figure 3.10 presents a detailed evaluation of model test set performances across different training set portions, ranging from 10% to 90%, using the optimal number of features identified for each model. This analysis was conducted simply to find out if changing the training set size dramatically affected the generalization performance of the model. Increasing the training set size almost always improved test performance. This improvement was expectedly sharper with fewer training data points and became increasingly shallow as the training set size increased and the test set size decreased. Figure 3.10 shows that a 90/10 split with 10-fold CV is optimal and acceptable for most of the best-performing models.

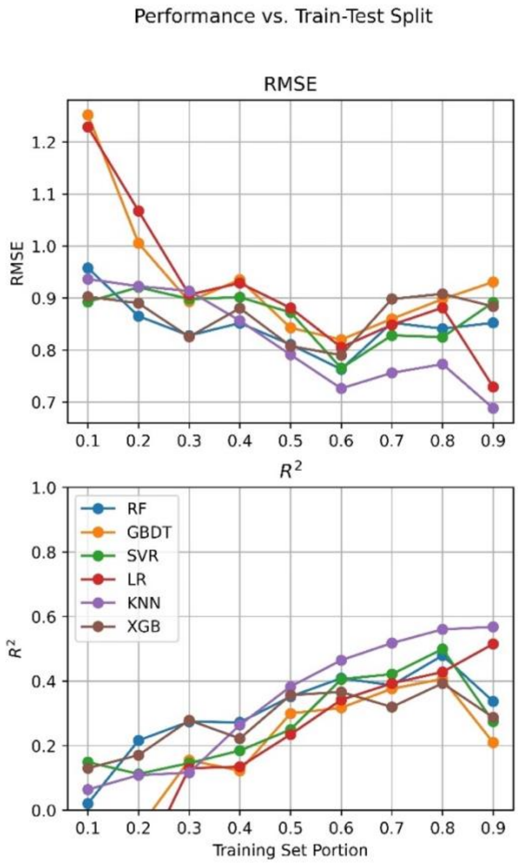

Figure 3.10 Effect of training set size on model performance.

Considering the analysis results presented in Table 3.12, the KNN model utilizing five features emerged as the most effective model. Figure 3.11 offers a detailed evaluation of the KNN model's performance through R^2 and RMSE metrics. The figure distinctly illustrates that the model performs optimally with a training set comprising 90% of the data and a test set of 10%. Consequently, the KNN model with eight features and a 90/10 train-test split was selected as the final model for predicting E_{corr} in this study. Figure 3.12 illustrates the regression performance of the KNN model.

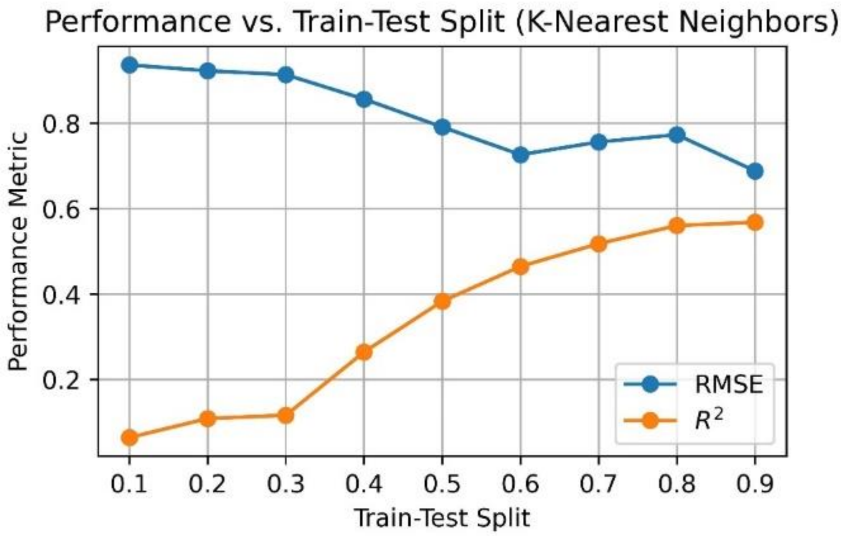

Figure 3.11 Figure offers a detailed evaluation of the KNN model's performance through R² and RMSE metrics

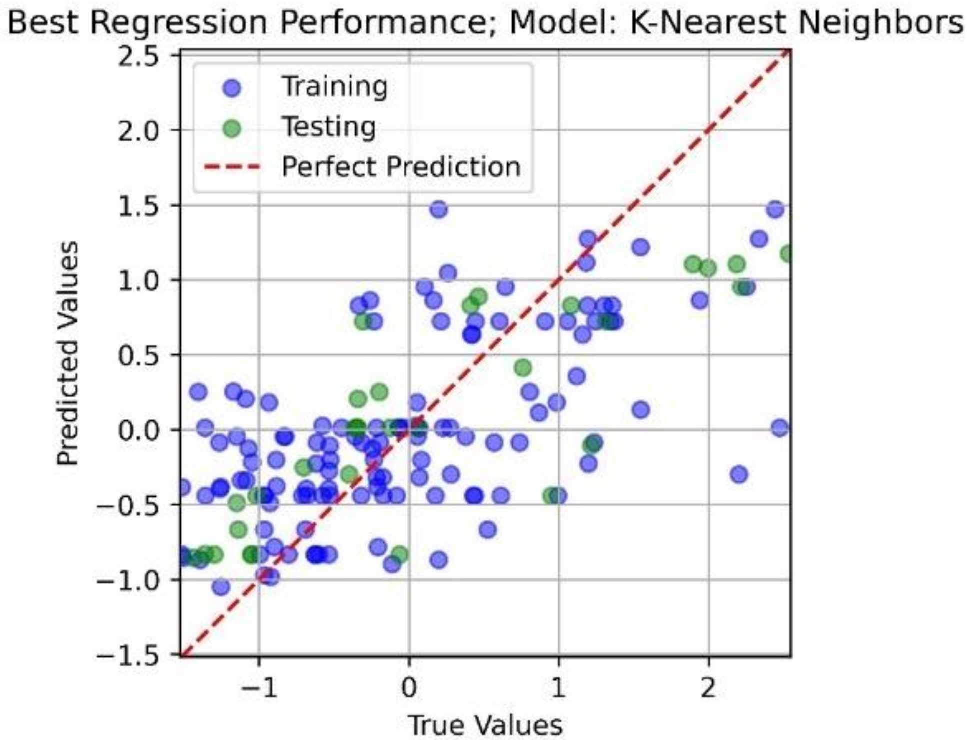

Figure 3.12 Regression performance of the KNN model

Following feature engineering and model training, the final step involved predicting the optimal NCF using the best-trained model. To achieve this, a synthetic dataset was generated, encompassing all possible quinary compositions of Ni and Ti, with Ni concentrations ranging from 48 at. % to 57 at. % in 0.03 at. % increments. These synthetic compositions were then fed into the machine learning model that demonstrated the best performance, enabling the prediction of the most favourable NCF value. Three of the best predicted compositions were selected for experimental validation, as detailed in Table 3.13

Table 3.13 Top three predicted NiTi compositions with the highest NCF values based on the best-performing machine learning model.

Ni at%	**Ti at%**	**Angle**	**Radius**	**Af**	**Heat Treatment**	**Predicted NCF**
48.36	51.64	60	5	45	1	954.0054545
48.72	51.28	60	5	26	1	928.2818182
48.27	51.73	60	5	10	1	905.4636364

Chapter 4:
DISCUSSION

This study aimed to determine the optimal NiTi alloy composition that maximizes cyclic fatigue resistance by combining experimental data with machine learning algorithms. Most studies investigating the cyclic fatigue resistance of endodontic files are limited to comparisons between a few commercially available brands. In addition to fatigue testing, studies that examine the microstructural characteristics of the instruments included in such research remain scarce. As a result, only general inferences can be made regarding which features contribute to greater fracture resistance. Existing evaluations typically rely on the overall design or manufacturing characteristics of the instruments, while direct comparisons based on material composition are lacking in the literature. This study aimed to address this gap by structurally characterizing the selected files using DSC and SEM-EDX, and systematically analysing the resulting data through machine learning. In this respect, the present study represents the first of its kind in the literature.

In this thesis, input parameters such as the Ni-Ti ratio and A_f value were not clearly available for all file brands. These details are typically not disclosed by manufacturers and are reported in only a limited number of studies. Therefore, SEM-EDX and DSC analyses were performed on the selected file brands prior to the machine learning phase in order to obtain these data. The findings obtained through SEM-EDX and DSC analyses in this study can be compared with those reported in previous studies that employed similar techniques to evaluate NiTi instruments.

In the present study, the A_f temperature of HyFlex EDM was found to be 53 °C, which is consistent with previously reported values in the literature. For example, Kimura et al. reported an A_f value of 49.9 °C, Elsewify et al. found 50 °C, Versiani et al. observed a considerably higher value of 56.8 °C, Kasuga et al. reported 54.7 °C, and Arias et al. documented 51.5 °C [65-69]. Although slight variations exist among studies, which may be attributed to differences in manufacturing batches or testing conditions, the overall agreement supports the reliability of the DSC measurement conducted in this study. The obtained A_f value confirms that HyFlex EDM exhibits a high transformation temperature, suggesting a predominantly martensitic structure at body temperature, which is in line with its known clinical behavior and flexibility.

The A_f value of ProTaper Universal was adopted as 11 °C, based on the data reported by Martins et al [41]. This decision was made since the file is no longer available on the market and direct analysis could not be performed. The chosen value is consistent with other findings in the literature, where Martins et al. reported A_f temperatures of 10.6 °C, 11.4 °C, and 11.7 °C [21, 70, 71], and Govindjee et al. found 11.3 °C [72]. This strong agreement among previous studies supports the validity of using 11 °C as the representative A_f value. The low transformation temperature is typical of conventional austenitic NiTi alloys.

ProTaper Gold exhibited an A_f temperature of 46.8 °C in this study. While this value is slightly lower than those reported in previous literature, such as 53 °C, 49 °C, and 47.7 °C by Martins et al. [21, 70, 71], and 50.6 °C by Hou et al.[73], it remains within an acceptable range for instruments that have undergone proprietary heat treatment. ProTaper Gold shares the same geometric design as ProTaper Universal but differs in its thermomechanical properties due to the additional heat treatment process. The relatively high Af value observed in this study confirms the shift from an austenitic structure toward a more martensitic or mixed-phase behavior at body temperature, which contributes to its increased flexibility and improved cyclic fatigue resistance.

The A_f temperature of ProTaper Next was measured as 45.5 °C in this study. This value is nearly identical to the 45.7 °C reported by Govindjee et al. [72], while slightly lower than the values reported by Gouédard (51 °C) and Hou (51.4 °C) [73, 74]. ProTaper Next is manufactured using M-Wire technology, which involves proprietary heat treatment to enhance flexibility while maintaining cutting efficiency. The measured A_f value suggests a partially martensitic structure at body temperature.

Among the instruments examined, Mtwo, One Curve, One Shape, VDW Rotate, and Revo-S have limited representation in the literature regarding transformation temperatures. For Mtwo, Kasuga et al. reported an A_f value of 15.7 °C [69], while the present study found a lower value of 10.6 °C, consistent with its classification as a conventional austenitic NiTi file. One Curve and One Shape are part of the same product line, with One Curve representing the heat-treated version of One Shape. Reported A_f values for One Curve range between 40 °C and 50 °C [75], and Azizi et al. documented 49 °C [23]; our result of 39.9 °C aligns with these findings. For One Shape, A_f values reported in the literature range from 10 °C to 19 °C [75], and the current measurement of 10.9 °C supports its identification as a non-heat-treated, austenitic instrument. VDW Rotate, which features a cross-sectional design similar to Mtwo but is thermally treated, showed an A_f temperature of 26.2 °C in this study. To the best of our knowledge, no previous data on the A_f value of VDW Rotate is available in the literature. Similarly, no transformation temperature data were found for Revo-S; in the present study, its A_f temperature was measured as 9.8 °C, suggesting an austenitic structure consistent with conventional NiTi instruments. Collectively, these findings illustrate the influence of heat treatment on the transformation behavior of endodontic files, even among instruments with similar geometries.

In most previous studies, the elemental composition of NiTi alloys has been reported without specific detail, using only the general term ‘near-equiatomic’ without providing exact atomic ratios [21, 23]. Only a limited number of investigations have reported specific values. One study analyzing HyFlex EDM reported a Ni:Ti ratio of 1.062, corresponding to 51.5% Ni and 48.5% Ti [68], while another reported a composition of 52.4% Ti and 47.6% Ni [76]. In the present study, the elemental analysis of HyFlex EDM revealed a composition of 51.47% Ti and 48.53% Ni.

In this study, the results obtained from SEM-EDX and DSC analyses were generally in agreement with the limited data available in the literature. Although minor differences were noted, the transformation temperatures and NiTi compositions showed overall consistency with previous findings. Since only a few studies have reported such detailed structural and thermal analyses of NiTi endodontic files, the data presented here offer valuable new insights. Moreover, these experimentally obtained parameters served as important inputs for the machine learning models, enabling a more systematic evaluation of the relationship between alloy composition and cyclic fatigue resistance.

Cyclic fatigue testing is not fully standardized, and results can be affected by a wide range of experimental variables [26]. While curvature angle and radius are commonly reported, other influential parameters, such as the length of the curvature, rotational speed, type of irrigation solution, or testing temperature, are frequently not reported. Hülsmann et al. highlighted this inconsistency in a review comparing results from different studies using the same file brand and size. For instance, the reported variation in cyclic fatigue resistance reached up to 39.7% for ProTaper Universal and an astonishing 636.4% for MTwo [26]. To reduce variability and increase the reliability of the input data, this study applied some inclusion criteria.

Although NiTi instruments are used inside the root canal system at body temperature, the majority of cyclic fatigue studies in the literature have been conducted at room temperature. As highlighted by Savitha et al., heat-treated instruments show significantly lower fatigue resistance at body temperature compared to room temperature [33]. However, due to the limited number of studies performed at body temperature, and to maintain consistency across the dataset, only studies conducted at room temperature were included in the present analysis.

Ashkar et al. analyzed 25 studies comparing the cyclic fatigue resistance of NiTi instruments used with continuous rotation and reciprocating motion. Their findings showed that reciprocating motion significantly improves fatigue resistance, taking into account factors such as taper, cross-sectional design, canal curvature, irrigation, and temperature. However, in the present study, only instruments with continuous rotation kinematics were included to ensure consistency in motion type across the dataset [77].

In addition, experimental setups involving double-curved or S-shaped canals, unclear or undefined curvature angles and radii, and combined fracture testing models (cyclic and torsional fatigue together) were excluded. Despite these efforts, some degree of heterogeneity may still be present among the included studies. Therefore, proper data preprocessing was applied to account for potential non-normal distributions and reduce the influence of outliers in the machine learning models.

Initially, the dataset contained a limited number of samples but a relatively high number of input features, which increased the risk of overfitting and reduced the model's generalizability. Therefore, feature selection techniques such as Pearson Correlation Coefficient and Random Forest-based importance ranking were applied to eliminate redundant, non-informative, or highly correlated variables. As a result, features like Ti, atomic mass, valence electron number, and electronegativity were excluded due to perfect correlation or lack of variance. The refined input set, consisting of only the most informative variables (e.g., Ni, A_f, Angle, Radius, and Heat Treatment), enabled the development of a more robust and interpretable model. This transformation not only reduced model complexity but also improved the overall predictive performance.

Gradient Boosted Decision Trees is a highly effective machine learning algorithm, especially known for its strong predictive performance and interpretability. Although a known limitation of GBDT is its inefficiency in handling multiple output variables since it constructs separate trees for each and ignores correlations between them, this drawback is not relevant to the present study [59]. As the current modelling task involves predicting a single output variable (NCF), GBDT can be used to its full potential without encountering such limitations. Therefore, GBDT was considered a suitable algorithm for this study due to its ability to handle single-output regression tasks efficiently.

At the initial stage of this study, the dataset included a relatively small number of observations compared to the number of features, representing a typical “low sample size, high dimensionality” scenario. In such cases, models that are less prone to overfitting and capable of handling high-dimensional input spaces are preferred. Random Forest (RF), being an ensemble method based on multiple decision trees, is well-suited for this purpose [78]. It performs well even when the feature space is large and provides internal estimates of feature importance, which is highly valuable for interpreting model outputs. For these reasons, the use of the Random Forest algorithm was considered appropriate in both the modelling and feature selection phases of this study.

One of SVR’s key advantages is its ability to handle high-dimensional data while maintaining stability in small sample settings and avoiding overfitting. These characteristics are especially valuable given the initial structure of the dataset, which had more features than samples. In this study, SVR demonstrated strong generalization capability and competitive performance on the test data. Although feature selection was applied to reduce dimensionality, SVR remained a suitable model due to its strong performance in small-sample regression tasks and its ability to model non-linear relationships through kernel functions [79]. For these reasons, SVR was chosen as a reliable and theoretically appropriate model for predicting NCF values.

Linear Regression was included in this study due to its simplicity, transparency, and usefulness as a baseline model. Although it may not capture complex nonlinear relationships like some advanced algorithms, it helps evaluate whether a linear relationship exists between the input features and the output (NCF) [80].

During the step-by-step feature inclusion process, SVR showed better performance than other models when only the top 4 features were used. This result reflects SVR's ability to perform well with small datasets that include a few highly informative variables. However, as more features were added, after including the top five, the KNN model started to show better generalization performance.

The change in model performance can be explained by how each algorithm works. SVR needs careful tuning as the number of features increases, because it becomes more sensitive to complexity. On the other hand, KNN relies on local patterns in the data and can benefit from having more features, especially if those features add useful and complementary information. With more input variables, KNN is better able to find similar data points and make accurate predictions.

KNN's non-parametric structure makes it less likely to overfit, especially in small or medium-sized datasets when proper validation is used. The improved performance of KNN after including five features suggests that combining compositional (Ni), geometric (Angle, Radius), and thermal (A_f, Heat Treatment) parameters gave a more complete view of the data. KNN was able to use this richer feature set more effectively. While SVR worked better in the early stages with fewer key features, KNN gave more accurate predictions when all features were included. This result shows how important it is to choose a model that matches the complexity and structure of the input data, especially in materials-related machine learning studies.

In the final part of the study, synthetic data were created to predict the best NiTi composition for improving NCF. Using small increments in composition made it possible to explore the design space in more detail than would be practical with experiments alone. Since KNN performed best with all selected features, it was used for these predictions.

Among the synthetic compositions evaluated, the top three predicted NCF values were associated with Ni concentrations ranging from 48.27 to 48.72 at.%, under constant canal geometry and heat treatment conditions. Notably, increasing A_f values were accompanied by higher predicted fatigue resistance, suggesting a positive correlation between phase transformation temperature and NCF. These findings are consistent with previous literature reporting improved cyclic fatigue resistance in files with higher A_f values, likely due to increased martensitic content at body temperature. Additionally, the predicted optimal compositions tended to be slightly Ti-rich, a condition known to increase A_f and promote a more martensitic structure at body temperature. This structural shift enhances flexibility and may contribute to the improved cyclic fatigue resistance observed in the predictions.

This study has some limitations to consider. Although the dataset included files with different designs, such as S-shaped and triangular cross-sections, these geometric features were not included as model inputs. In reality, factors such as cross-sectional shape, pitch design, rake angle, and cutting length can impact cyclic fatigue resistance. Another limitation is the lack of experimental validation for the predicted optimal compositions, which would be necessary for confirming the results. Future studies should also expand the dataset by including files with different sizes and design characteristics, and combine modelling with mechanical testing.

Chapter 5:
CONCLUSION

This study aimed to predict the optimal NiTi alloy composition for maximizing the cyclic fatigue resistance of endodontic rotary instruments by integrating experimental characterization with machine learning techniques. DSC and SEM-EDX analyses were performed on a selected set of NiTi files to determine their thermal and compositional properties. With this approach, this study contributed to the limited data available on the compositional and thermal properties of these instruments and provided a dataset suitable for machine learning applications. After feature selection, several machine learning models were tested, and the K-Nearest Neighbors (KNN) algorithm yielded the most accurate predictions when all relevant features, including composition, thermal behavior, and canal geometry, were considered. A synthetic dataset was then generated to explore the design space, and the top three predicted compositions were identified as potential candidates for enhanced fatigue resistance. While experimental validation remains a necessary future step, this study represents an initial step toward data-driven modelling based on material properties in the context of endodontic instrument design. In future work, the inclusion of additional design-related and mechanical features may allow for more comprehensive predictions.

BIBLIOGRAPHY

[1] S. Zinelis, T. Eliades, and G. Eliades, "A metallurgical characterization of ten endodontic Ni-Ti instruments: assessing the clinical relevance of shape memory and superelastic properties of Ni-Ti endodontic instruments," *International endodontic journal,* vol. 43, no. 2, pp. 125-134, 2010.

[2] M. Revathi, C. Rao, and L. Lakshminarayanan, "Revolutions in endodontic instruments-a review," *Endodontology,* vol. 13, no. 2, pp. 43-50, 2001.

[3] L. N. Rao, S. L. Thirunarayanan, and A. Shetty, "Impact of a retained instrument on treatment outcome: A systematic review," *Journal of Health and Allied Sciences NU,* vol. 13, no. 02, pp. 168-171, 2023.

[4] H. Zhou, B. Peng, and Y. F. Zheng, "An overview of the mechanical properties of nickel–titanium endodontic instruments," *Endodontic topics,* vol. 29, no. 1, pp. 42-54, 2013.

[5] V. Faus-Llácer, N. H. Kharrat, C. Ruiz-Sánchez, I. Faus-Matoses, Á. Zubizarreta-Macho, and V. Faus-Matoses, "The effect of taper and apical diameter on the cyclic fatigue resistance of rotary endodontic files using an experimental electronic device," *Applied Sciences,* vol. 11, no. 2, p. 863, 2021.

[6] M. A. Versiani, B. Basrani, and M. D. Sousa-Neto, "The root canal anatomy in permanent dentition," Springer, 2019.

[7] G. V. Black, *Descriptive anatomy of the human teeth*. SS White manufacturing Company, 1897.

[8] O. A. Peters, G. Rossi-Fedele, R. George, K. Kumar, A. Timmerman, and P. P. Wright, "Guidelines for non-surgical root canal treatment," ed: Wiley Online Library, 2024.

[9] M. Versiani, J. Martins, and R. Ordinola-Zapata, "Anatomical complexities affecting root canal preparation: a narrative review," *Australian dental journal,* vol. 68, pp. S5-S23, 2023.

[10] L. H. Berman and K. M. Hargreaves, *Cohen's Pathways of the Pulp-E-Book: Cohen's Pathways of the Pulp-E-Book*. Elsevier Health Sciences, 2020.

[11] S. Buchanan, "New additions to the NiTi rotary file market: What to bring in and what to leave out," *Dental Tribune U.S. Edition,* vol. 6, pp. 19-20, 2011.

[12] G. De Deus, E. J. Silva, E. Souza, M. A. Versiani, and M. Zuolo, *Shaping for cleaning the root canals: a clinical-based strategy*. Springer Nature, 2021.

[13] W. J. Buehler, J. V. Gilfrich, and R. C. Wiley, "Effect of low-temperature phase changes on the mechanical properties of alloys near composition TiNi," *Journal of applied physics,* vol. 34, no. 5, pp. 1475-1477, 1963.

[14] G. F. Andreasen and R. E. Morrow, "Laboratory and clinical analyses of nitinol wire," *American journal of orthodontics,* vol. 73, no. 2, pp. 142-151, 1978.

[15] S. Civjan, E. F. Huget, and L. B. DeSimon, "Potential applications of certain nickel-titanium (nitinol) alloys," *Journal of dental research,* vol. 54, no. 1, pp. 89-96, 1975.

[16] M. Haapasalo and Y. Shen, "Evolution of nickel–titanium instruments: from past to future," *Endodontic topics,* vol. 29, no. 1, pp. 3-17, 2013.

[17] Y. Oshida and T. Tominaga, *Nickel-titanium materials: biomedical applications*. Walter de Gruyter GmbH & Co KG, 2020.

[18] G. Yared, "Canal preparation using only one Ni-Ti rotary instrument: preliminary observations," *International endodontic journal,* vol. 41, no. 4, pp. 339-344, 2008.
[19] J. Frenzel, E. P. George, A. Dlouhy, C. Somsen, M.-X. Wagner, and G. Eggeler, "Influence of Ni on martensitic phase transformations in NiTi shape memory alloys," *Acta Materialia,* vol. 58, no. 9, pp. 3444-3458, 2010.
[20] K. Otsuka and X. Ren, "Physical metallurgy of Ti–Ni-based shape memory alloys," *Progress in materials science,* vol. 50, no. 5, pp. 511-678, 2005.
[21] J. N. Martins *et al.*, "Comparison of five rotary systems regarding design, metallurgy, mechanical performance, and canal preparation—A multimethod research," *Clinical Oral Investigations,* vol. 26, no. 3, pp. 3299-3310, 2022.
[22] J. N. Martins *et al.*, "A Comparative Analysis of ProTaper Ultimate and Five Multifile Systems: Design, Metallurgy, and Mechanical Performance," *Materials,* vol. 18, no. 6, p. 1260, 2025.
[23] A. Azizi *et al.*, "In-depth metallurgical and microstructural analysis of OneShape and heat treated OneCurve instruments," *European endodontic journal,* vol. 6, no. 1, p. 90, 2021.
[24] Y. Shen and M. Haapasalo, "Nickel-Titanium Metallurgy," *Endodontic Advances and Evidence-Based Clinical Guidelines,* pp. 268-282, 2022.
[25] S. Thompson, "An overview of nickel–titanium alloys used in dentistry," *International endodontic journal,* vol. 33, no. 4, pp. 297-310, 2000.
[26] M. Hülsmann, D. Donnermeyer, and E. Schäfer, "A critical appraisal of studies on cyclic fatigue resistance of engine-driven endodontic instruments," *International endodontic journal,* vol. 52, no. 10, pp. 1427-1445, 2019.
[27] M. McGuigan, C. Louca, and H. Duncan, "Endodontic instrument fracture: causes and prevention," *British dental journal,* vol. 214, no. 7, pp. 341-348, 2013.
[28] Y. Shen and G. S. Cheung, "Methods and models to study nickel–titanium instruments," *Endodontic topics,* vol. 29, no. 1, pp. 18-41, 2013.
[29] A. Jamleh *et al.*, "Endodontic instruments after torsional failure: nanoindentation test," *Scanning: The Journal of Scanning Microscopies,* vol. 36, no. 4, pp. 437-443, 2014.
[30] J. P. Pruett, D. J. Clement, and D. L. Carnes Jr, "Cyclic fatigue testing of nickel-titanium endodontic instruments," *Journal of endodontics,* vol. 23, no. 2, pp. 77-85, 1997.
[31] H. Topçuoğlu, G. Topçuoğlu, Ö. Kafdağ, and H. Arslan, "Cyclic fatigue resistance of new reciprocating glide path files in 45-and 60-degree curved canals," *International endodontic journal,* vol. 51, no. 9, pp. 1053-1058, 2018.
[32] A. Dosanjh, S. Paurazas, and M. Askar, "The effect of temperature on cyclic fatigue of nickel-titanium rotary endodontic instruments," *Journal of endodontics,* vol. 43, no. 5, pp. 823-826, 2017.
[33] S. Savitha, S. Sharma, V. Kumar, A. Chawla, P. Vanamail, and A. Logani, "Effect of body temperature on the cyclic fatigue resistance of the nickel–titanium endodontic instruments: A systematic review and meta-analysis of: in vitro: studies," *Journal of Conservative Dentistry and Endodontics,* vol. 25, no. 4, pp. 338-346, 2022.
[34] Ü. K. Bulem, A. D. Kececi, and H. E. Guldas, "Experimental evaluation of cyclic fatigue resistance of four different nickel-titanium instruments after immersion in sodium hypochlorite and/or sterilization," *Journal of Applied Oral Science,* vol. 21, no. 6, pp. 505-510, 2013.

[35] S. W. Schneider, "A comparison of canal preparations in straight and curved root canals," *Oral surgery, Oral medicine, Oral pathology,* vol. 32, no. 2, pp. 271-275, 1971.
[36] D. Di Nardo *et al.*, "Influence of different cross-section on cyclic fatigue resistance of two nickel–titanium rotary instruments with same heat treatment: An: in vitro: study," *Saudi Endodontic Journal,* vol. 10, no. 3, pp. 221-225, 2020.
[37] N. Grande, G. Plotino, R. Pecci, R. Bedini, V. A. Malagnino, and F. Somma, "Cyclic fatigue resistance and three-dimensional analysis of instruments from two nickel–titanium rotary systems," *International endodontic journal,* vol. 39, no. 10, pp. 755-763, 2006.
[38] R. He and J. Ni, "Design improvement and failure reduction of endodontic files through finite element analysis: application to V-Taper file designs," *Journal of Endodontics,* vol. 36, no. 9, pp. 1552-1557, 2010.
[39] M. Maroof, R. Sujithra, and R. P. Tewari, "Superelastic and shape memory equi-atomic nickel-titanium (Ni-Ti) alloy in dentistry: a systematic review," *Materials Today Communications,* vol. 33, p. 104352, 2022.
[40] Y. Shen, H.-m. Zhou, Y.-f. Zheng, B. Peng, and M. Haapasalo, "Current challenges and concepts of the thermomechanical treatment of nickel-titanium instruments," *Journal of endodontics,* vol. 39, no. 2, pp. 163-172, 2013.
[41] J. N. Martins *et al.*, "Mechanical performance and metallurgical features of ProTaper Universal and 6 replicalike systems," *Journal of Endodontics,* vol. 46, no. 12, pp. 1884-1893, 2020.
[42] A. Zanza, M. Seracchiani, R. Reda, G. Miccoli, L. Testarelli, and D. Di Nardo, "Metallurgical tests in endodontics: a narrative review," *Bioengineering,* vol. 9, no. 1, p. 30, 2022.
[43] E. J. Silva *et al.*, "Mechanical tests, metallurgical characterization, and shaping ability of nickel-titanium rotary instruments: a multimethod research," *Journal of Endodontics,* vol. 46, no. 10, pp. 1485-1494, 2020.
[44] V. Sekar, R. Kumar, S. Nandini, S. Ballal, and N. Velmurugan, "Assessment of the role of cross section on fatigue resistance of rotary files when used in reciprocation," *European journal of dentistry,* vol. 10, no. 04, pp. 541-545, 2016.
[45] S. B. Alapati *et al.*, "Metallurgical characterization of a new nickel-titanium wire for rotary endodontic instruments," *Journal of endodontics,* vol. 35, no. 11, pp. 1589-1593, 2009.
[46] H. Lu *et al.*, "Simultaneous enhancement of mechanical and shape memory properties by heat-treatment homogenization of Ti2Ni precipitates in TiNi shape memory alloy fabricated by selective laser melting," *Journal of Materials Science & Technology,* vol. 101, pp. 205-216, 2022.
[47] P. Pattanaik *et al.*, "Comparative Evaluation of the Shaping Ability of the Recent, Fifth-generation ProTaper Next and Revo-S NiTi Rotary Endodontic Files Using Three-dimensional Imaging: An Imaging-based Study," *Journal of Microscopy and Ultrastructure,* p. 10.4103, 2023.
[48] A. Guelzow, O. Stamm, P. Martus, and A. Kielbassa, "Comparative study of six rotary nickel–titanium systems and hand instrumentation for root canal preparation," *International endodontic journal,* vol. 38, no. 10, pp. 743-752, 2005.
[49] J.-G. Kim, K.-Y. Kum, and E.-S. Kim, "Comparative study on morphology of cross-section and cyclic fatigue test with different rotary NiTi files and handling methods," *Journal of Korean Academy of Conservative Dentistry,* vol. 31, no. 2, pp. 96-102, 2006.

[50] J. Zupanc, N. Vahdat-Pajouh, and E. Schäfer, "New thermomechanically treated NiTi alloys–a review," *International endodontic journal,* vol. 51, no. 10, pp. 1088-1103, 2018.
[51] X. Xu, M. Eng, Y. Zheng, and D. Eng, "Comparative study of torsional and bending properties for six models of nickel-titanium root canal instruments with different cross-sections," *Journal of Endodontics,* vol. 32, no. 4, pp. 372-375, 2006.
[52] P. M. Venino, C. L. Citterio, A. Pellegatta, M. Ciccarelli, and M. Maddalone, "A micro–computed tomography evaluation of the shaping ability of two nickel-titanium instruments, HyFlex EDM and ProTaper next," *Journal of endodontics,* vol. 43, no. 4, pp. 628-632, 2017.
[53] J. Bhagyaraj, K. Ramaiah, C. Saikrishna, and S. Bhaumik, "Behavior and effect of Ti2Ni phase during processing of NiTi shape memory alloy wire from cast ingot," *Journal of alloys and compounds,* vol. 581, pp. 344-351, 2013.
[54] W. Huang, P. Martin, and H. L. Zhuang, "Machine-learning phase prediction of high-entropy alloys," *Acta Materialia,* vol. 169, pp. 225-236, 2019.
[55] E. F. Morales and H. J. Escalante, "A brief introduction to supervised, unsupervised, and reinforcement learning," in *Biosignal processing and classification using computational learning and intelligence*: Elsevier, 2022, pp. 111-129.
[56] S. K. Chinnamgari, *R Machine Learning Projects: Implement supervised, unsupervised, and reinforcement learning techniques using R 3.5*. Packt Publishing Ltd, 2019.
[57] M. K. Uçar, M. Nour, H. Sindi, and K. Polat, "The effect of training and testing process on machine learning in biomedical datasets," *Mathematical Problems in Engineering,* vol. 2020, no. 1, p. 2836236, 2020.
[58] G. Biau and E. Scornet, "A random forest guided tour," *Test,* vol. 25, no. 2, pp. 197-227, 2016.
[59] Z. Zhang and C. Jung, "GBDT-MO: Gradient-boosted decision trees for multiple outputs," *IEEE transactions on neural networks and learning systems,* vol. 32, no. 7, pp. 3156-3167, 2020.
[60] D. Maulud and A. M. Abdulazeez, "A review on linear regression comprehensive in machine learning," *Journal of applied science and technology trends,* vol. 1, no. 2, pp. 140-147, 2020.
[61] A. Gupta, A. Sharma, and A. Goel, "Review of regression analysis models," *Int. J. Eng. Res. Technol,* vol. 6, no. 08, pp. 58-61, 2017.
[62] K. Taunk, S. De, S. Verma, and A. Swetapadma, "A brief review of nearest neighbor algorithm for learning and classification," in *2019 international conference on intelligent computing and control systems (ICCS)*, 2019: IEEE, pp. 1255-1260.
[63] Z. A. Ali, Z. H. Abduljabbar, H. A. Tahir, A. B. Sallow, and S. M. Almufti, "eXtreme gradient boosting algorithm with machine learning: A review," *Academic Journal of Nawroz University,* vol. 12, no. 2, pp. 320-334, 2023.
[64] S. S. Azmi and S. Baliga, "An overview of boosting decision tree algorithms utilizing AdaBoost and XGBoost boosting strategies," *Int. Res. J. Eng. Technol,* vol. 7, no. 5, pp. 6867-6870, 2020.
[65] A. Arias, J. C. Macorra, S. Govindjee, and O. A. Peters, "Correlation between temperature-dependent fatigue resistance and differential scanning calorimetry

analysis for 2 contemporary rotary instruments," *Journal of Endodontics,* vol. 44, no. 4, pp. 630-634, 2018.

[66] T. Elsewify, H. Elhalabi, and B. Eid, "Dynamic cyclic fatigue and differential scanning calorimetry analysis of R-Motion," *international dental journal,* vol. 73, no. 5, pp. 680-684, 2023.

[67] S. Kimura *et al.*, "Phase transformation behavior and mechanical properties of HyFlex EDM nickel-titanium endodontic rotary instrument: Evaluation at body temperature," *Journal of Dental Sciences,* vol. 19, no. 2, pp. 929-936, 2024.

[68] M. Versiani, "Multimethod analysis of three rotary instruments produced by electric discharge machining technology."

[69] Y. Kasuga *et al.*, "Temperature-dependent phase composition and mechanical properties of heat-treated nickel-titanium rotary endodontic instruments at room and body temperatures," 2023.

[70] J. N. Martins *et al.*, "Design, metallurgical features, and mechanical behavior of NiTi endodontic instruments from five different heat-treated rotary systems," *Materials,* vol. 15, no. 3, p. 1009, 2022.

[71] J. N. Martins *et al.*, "Characterization of the file-specific heat-treated ProTaper Ultimate rotary system," *International endodontic journal,* vol. 56, no. 4, pp. 530-542, 2023.

[72] R. Govindjee and S. Govindjee, "Thermal phase transformations in commercial dental files," 2015.

[73] X.-M. Hou, Y.-J. Yang, and J. Qian, "Phase transformation behaviors and mechanical properties of NiTi endodontic files after gold heat treatment and blue heat treatment," *Journal of Oral Science,* vol. 63, no. 1, pp. 8-13, 2021.

[74] C. Gouédard *et al.*, "Elements for understanding the bending and cyclic fatigue behavior of endodontic instruments," *Journal of Materials Engineering and Performance,* vol. 31, no. 5, pp. 3943-3952, 2022.

[75] S. Staffoli *et al.*, "Influence of environmental temperature, heat-treatment and design on the cyclic fatigue resistance of three generations of a single-file nickel–titanium rotary instrument," *Odontology,* vol. 107, pp. 301-307, 2019.

[76] T. Türk, C. Keskin, D. Çetin, and Ö. S. Yılmaz, "Multimethod assessment of design, mechanical and metallurgical characteristics of ProTaper Ultimate, TruNatomy Glider, ProGlider, Hyflex EDM and WaveOne Gold Glider glide path instruments," *Odontology,* pp. 1-12, 2025.

[77] I. Ashkar, J. L. Sanz, and L. Forner, "Cyclic fatigue resistance of glide path rotary files: a systematic review of in vitro studies," *Materials,* vol. 15, no. 19, p. 6662, 2022.

[78] K. J. Archer and R. V. Kimes, "Empirical characterization of random forest variable importance measures," *Computational statistics & data analysis,* vol. 52, no. 4, pp. 2249-2260, 2008.

[79] F. Zhang and L. J. O'Donnell, "Support vector regression," in *Machine learning*: Elsevier, 2020, pp. 123-140.

[80] N. Roustaei, "Application and interpretation of linear-regression analysis," *Medical Hypothesis, Discovery and Innovation in Ophthalmology,* vol. 13, no. 3, p. 151, 2024.